

1 The manuscript was submitted to the journal *Sedimentary Geology*, on Dec. 21<sup>st</sup>, 2020, and  
2 it was accepted for publication on Mar. 10<sup>th</sup>, 2021:

3 (The DOI of published article: <https://doi.org/10.1016/j.sedgeo.2021.105901> )  
4

## 5 **Polygenetic mélange in the retrowedge foredeep of an active arc-** 6 **continent collision, Coastal Range of eastern Taiwan**

7  
8 Larry Syu-Heng Lai<sup>a</sup>, Rebecca J. Dorsey<sup>a</sup>, Chorng-Shern Horng<sup>b</sup>, Wen-Rong Chi<sup>cd</sup>, Kai-Shuan Shea<sup>e</sup>, Jiun-  
9 Yee Yen<sup>f</sup>

10  
11 <sup>a</sup>*Department of Earth Sciences, University of Oregon, Eugene, Oregon 97403, United States*

12 <sup>b</sup>*Institute of Earth Sciences, Academia Sinica, Taipei 11529, Taiwan*

13 <sup>c</sup>*Department of Earth Sciences, National Cheng Kung University, Tainan 701, Taiwan*

14 <sup>d</sup>*Department of Earth Sciences, National Central University, Taoyuan 320, Taiwan.*

15 <sup>e</sup>*Central Geological Survey, Ministry of Economic Affairs, New Taipei 235, Taiwan*

16 <sup>f</sup>*Department of Natural Resources and Environmental Studies, National Dong Hwa University, Hualien*  
17 *97401, Taiwan*

18  
19 \*Corresponding author: Larry Syu-Heng Lai ([larrysyuhenglai@gmail.com](mailto:larrysyuhenglai@gmail.com))  
20

### 21 **Abstract**

22 The Plio-Pleistocene Lichi Mélange in the Coastal Range of eastern Taiwan offers an excellent  
23 opportunity to study processes of mélange development at the continent-ocean interface of an active arc-  
24 continent collision. This paper presents new results of detailed geologic mapping, lithofacies analysis,  
25 magneto-biostratigraphy, paleocurrent, and paleoslope analyses in the southern Coastal Range to investigate  
26 the origins and significance of this mélange. The results show that the Lichi Mélange consists of mass-transport  
27 deposits including well-stratified block-in-matrix beds (olistostromes), extra-formational blocks (olistoliths),  
28 and broken formation with abundant soft-sediment deformation features that transition laterally into distal

29 mega-slump beds and pebbly mudstones (subaqueous debrites). Abundant observations of depositional  
30 contacts and interbedding of mélangé with contemporary (ca. 4–1 Ma) flysch units of the Fanshuliao and  
31 Paliwan formations confirm their sedimentary origin. Compacted sedimentological shear fabrics in  
32 olistostromal facies are broadly parallel to internal stratification and bedding, and are readily distinguishable  
33 from cross-cutting brittle fault zones related to post ~1 Ma west-vergent thrust faults. Paleoslope and  
34 paleocurrent analyses record down-slope gravity-driven transport toward the east and southeast.

35 The data provide evidence for a polygenetic origin of the Lichi Mélangé, in which sedimentary mass-  
36 wasting deposits are overprinted by younger tectonic shear zones. Slide blocks, conglomerate clasts, and  
37 detrital sand were all derived from an eroding source in the east-vergent eastern retrowedge of the Taiwan  
38 collisional orogen. The source area included tectonically accreted fragments of the two converging plates that  
39 represent shallow-crustal equivalents of the Miocene Yuli Belt and Eastern Slates exposed in the modern  
40 Central Range. Reconstructed stratigraphic panels record eastward progradation of olistostromal facies over  
41 distal basinal flysch deposits, which we infer resulted from eastward (oceanward) migration of a steep  
42 submarine slope at the leading edge of the retrowedge orogenic front. Thus, the Coastal Range basin evolved  
43 as a migrating retro-foredeep basin that formed on top of older, pre-collisional volcanic arc and forearc crust.  
44 These results demonstrate a unique type of sedimentary basin that is formed and then rapidly inverted at a  
45 convergent continent-ocean interface during the transition from intra-oceanic subduction to arc-continent  
46 collision. This revised history of the Lichi Mélangé provides a new perspective on the dynamics of rapid crustal  
47 mixing and tectonic recycling at the convergent suture of an active arc-continent collision system.

48

#### 49 **Keywords**

50 Arc-Continent Collision, Taiwan Coastal Range, Lichi Mélangé, Olistostrome, Retrowedge foredeep basin

51



52 **1. Introduction**

53 “Mélange” in geology is a non-genetic lithological term defined as a mappable and chaotic rock unit  
54 consisting of extra-formational (exotic) blocks embedded in highly mixed and disrupted matrix (i.e., block-in-  
55 matrix fabrics) (Greenly, 1919; Hsü, 1968; Cowan, 1985). Mélanges form by large-scale stratal disruption via  
56 tectonic, diapiric, or sedimentary processes, or a combination of these processes (i.e., polygenetic) (Raymond,  
57 1984, 2019). They provide insights into the kinematics of crustal deformation and rock mixing at active plate  
58 margins, and therefore are useful for reconstructing continental growth over deep time in tectonically active  
59 settings (Dilek et al., 2012). Processes of mélangé formation at the continent-ocean interface of arc-continent  
60 collision zones are particularly controversial and poorly understood due to the relative paucity of well-  
61 preserved mélangé records from ancient arc-continent collision zones globally (e.g., Festa et al., 2010), despite  
62 a few recent advances in a Neoproterozoic arc-continent collision system of the North China Craton (e.g., Wang  
63 et al., 2019; Kusky et al., 2020). The low preservation potential of mélanges at suture zones likely reflects the  
64 short lifetime (often ~5-15 Myr) of arc-continent collision systems and rapid crustal erosion that occurs after  
65 the forearc crust is accreted in the retrowedge of arc-continent collision suture zones (Draut and Clift, 2013).

66 To address these challenges, many studies have focused on active arc-continent collision orogens  
67 where young or active mélangé generation can be directly observed (e.g., Harris and Audley-Charles, 1987;  
68 Huang et al., 2000). However, the genesis of these mélangé units remains debated in part due to inconsistent  
69 definitions of “mélangé” that lie at the center of controversies over tectonic models in many orogenic belts  
70 (Festa et al., 2012; Raymond, 2019). Growing evidence suggests that microscopic to outcrop-scale internal  
71 shears and block-in-matrix fabrics cannot be used as definitive criteria to distinguish mélangé formation by  
72 faulting, diapirism, or gravitational processes (Raymond, 1984; Ogata et al., 2012; Wakabayashi, 2019),  
73 because mechanical styles of stratal disruption and brecciation depend on local physical properties (e.g.,  
74 permeability, strength), which in turn depend on degree of consolidation, fluid content, pressure, temperature,  
75 and rate of structural loading and deposition (Michiguchi et al., 2011; Ogata et al., 2014; Festa et al., 2019). In

76 addition, recycling and incorporation of juvenile crustal materials via episodic tectonic and/or sedimentary  
77 processes commonly overprint older features at the boundary between advancing orogenic fronts and adjacent  
78 sedimentary basins (Festa et al., 2016; Moore et al., 2019; Ogata et al., 2019a). As such, interdisciplinary  
79 constraints from geologic mapping, stratigraphic analysis, kinematic study, etc. are required to advance our  
80 understanding of mélangé formation in arc-continent collision zones.

81 The Lichi Mélangé in the Coastal Range of eastern Taiwan (**Fig. 1**) is widely considered a classic  
82 example of mélangé formed in an arc-continent collision suture, but its origin is poorly understood and thus  
83 still a matter of debate (**Fig. 2**). Prior studies have documented evidence in support of both sedimentologic  
84 (e.g., Liou et al., 1977; Page and Suppe, 1981) and tectonic (e.g., Chen, 1997b; Chang et al., 2000, 2001)  
85 processes of rock mixing, suggesting a possible polygenetic origin for the Lichi Mélangé. However, the  
86 question of whether tectonic shearing or sedimentary (olistostromal) emplacement was the primary mode of  
87 shearing to form the Lichi Mélangé remains unresolved. Such controversy is related to alternate models for  
88 basin evolution recorded by Plio-Pleistocene sedimentary rocks in the Coastal Range. According to the  
89 prevailing hypothesis (**Fig. 2A**), the Coastal Range is underlain by relatively little-deformed volcanic islands  
90 and adjacent forearc, intra-arc, and backarc basins (e.g., Teng, 1987; Huang et al., 1995; Chen, 1997a; Song  
91 and Lo, 2002), and the Lichi Mélangé formed by tectonic shearing in a mega-thrust belt during large-scale  
92 forearc shortening (Chen, 1997b; Chang et al., 2001; Huang et al., 2008, 2018). Other studies suggest an  
93 olistostromal origin for the Lichi Mélangé and consider the main body of the mélangé to be part of a genetically  
94 related sedimentary sequence (e.g., Liou et al., 1977; Page and Suppe, 1981; Barrier and Muller, 1984) that  
95 filled a syn-orogenic flysch basin and was later tectonically inverted (e.g., Dorsey, 1988; Lundberg and Dorsey,  
96 1988) (**Fig. 2B**). The second hypothesis postulates that the basin is deformed by large thrust faults due to strong  
97 crustal shortening, and the modern topography of the Coastal Range reflects the areal distribution of young  
98 structures and antiformal culminations rather than intact volcanic islands (Dorsey, 1992; Thomas et al., 2014).

99           The origin of the Lichi Mélange is likely also related to the formation of the late-Miocene Yuli Belt,  
100 an exhumed greenschist-blueschist facies metamorphosed mélangé in the Central Range of Taiwan, located  
101 directly west of the Coastal Range (**Fig. 1A**). Recent studies of the Yuli Belt propose numerous tectonic models  
102 to explain mélangé formation and rapid exhumation at the collisional plate suture (e.g., Chen, W.-S. et al.,  
103 2017; Conand et al., 2020). Thus the Lichi Mélange sits at the center of ongoing debate over processes of  
104 mélangé formation during accretion of oceanic arc crust, mechanisms of tectonic recycling in arc-continent  
105 collision suture zones, and processes that drive growth of continental lithosphere through time (Clift and  
106 Vannucchi, 2004). High-resolution age constraints, geologic mapping, process-based sedimentology, and  
107 stratigraphic studies are therefore needed to resolve long-standing uncertainty and debate over the origins of  
108 the Lichi Mélange.

109           For this study we conducted detailed geologic mapping, lithofacies analysis, measured sections,  
110 magneto-biostratigraphy, paleoslope and paleocurrent analyses to test hypotheses for sedimentary versus  
111 tectonic origins of the Lichi Mélange. The results are systematically compiled below and applied to interpret  
112 the basin-filling history, reconstruct basin geometry, and evaluate the role of the Lichi Mélange in the evolution  
113 of the Taiwan collisional orogen.

114

## 115 **2. Geological background**

116           The island of Taiwan is an active arc-continent collisional orogen produced by oblique convergence  
117 between the Eurasian continental margin and Luzon Arc on the Philippine Sea plate (**Fig. 1**) (Suppe, 1984; Yu  
118 et al., 1997). The orogen is characterized by a low gradient west-vergent prowedge thrust belt in the west and  
119 a steep east-vergent retrowedge in the east, separated by a high drainage divide that parallels the major  
120 structural fabrics (Fisher et al., 2007). The major morphotectonic units of Taiwan include: (1) Pliocene to  
121 modern pro-foreland basin and west-vergent thrust belt in the western Taiwan Strait, Coastal Plain, and  
122 Western Foothills; (2) deformed low-grade Eocene to Miocene meta-sandstone and argillite in the Hsueshan

123 Range and western Central Range; (3) older metamorphic continental basement in the Tailuko Belt; (4)  
124 greenschist-blueschist facies mafic to ultramafic metamorphic rocks and associated meta-sediments in the  
125 eastern Central Range (Yuli Belt and Eastern Slates); and (5) accreted volcanic rocks of the Luzon Arc and  
126 overlying deformed sequence of unmetamorphosed flysch deposits in the Coastal Range (Teng, 1990; Chen,  
127 W.-S. et al., 2017). Estimates for the age of onset of collisional mountain building in Taiwan vary from about  
128 6.5 to 12.5 Ma based on stratigraphic evidence for flexural loading in the pro-foreland basin and earliest  
129 introduction of continental material into the trench (e.g., Lin et al., 2003; Tensi et al., 2006; Chen et al., 2019).  
130 Despite these differences, it is widely agreed that major orogenic uplift, crustal thickening and tectonic  
131 exhumation began at ca. 5 Ma. Pulses of accelerated exhumation occurred at ca. 1.5–2.0 Ma and 0.5 Ma as  
132 indicated by abrupt changes in sedimentation rate and sandstone petrography in syn-orogenic basins (Dorsey,  
133 1988; Teng, 1990; Nagel et al., 2014; Chen et al., 2019), timing of pressure-temperature dependent  
134 metamorphism (Beysac et al., 2008; Sandmann et al., 2015; Keyser et al., 2016), and bedrock cooling history  
135 based on thermochronologic studies (Lee et al., 2015; Hsu et al., 2016).

136 Previous studies of the Coastal Range have applied conflicting definitions of lithostratigraphic units  
137 (e.g., Horng and Shea, 1996; Chen, 2009; Huang et al., 2018; Lai, L.S.-H. et al., 2018), regional structures  
138 (e.g., Chen, W.-H. et al., 2015; Lai and Teng, 2016), and basin style and geometry (e.g., Teng, 1987; Lundberg  
139 and Dorsey, 1988; Huang et al., 1995; Chen et al., 2019). In addition, the term “mélange” has been defined  
140 differently in published analyses and geologic maps (e.g., Hsu, 1956; Page and Suppe, 1981; Barrier and  
141 Muller, 1984; Chen, 1997b; Chang et al., 2000; Chen, W.-H. et al., 2017; Huang et al., 2018), resulting in  
142 ambiguous tectonic interpretations for eastern Taiwan. In the following sections, we present a standardized  
143 lithostratigraphic framework and rock classification scheme for coherent (non-mélange) strata in the Coastal  
144 Range based on a synthesis of classic and recent published studies. We then summarize existing knowledge of  
145 regional structures in the southern Coastal Range, current models for the Lichi Mélange and basin evolution,  
146 and provide standard definitions and stratigraphic nomenclature to be used in this paper.

147

148 *2.1. Non-mélange strata and structures of the Coastal Range*

149 Miocene rocks representing arc and forearc crust in the Coastal Range are unconformably overlain by  
150 a thick (4-7 km) section of Plio-Pleistocene synorogenic marine flysch and conglomerate (**Fig. 3**). The  
151 Tuluanshan Formation is defined as all volcanic and volcanoclastic rocks beneath the unconformity, including  
152 the Chimei Igneous Complex (~15–9 Ma), Shihmen Volcanic Breccia, and older Shihtiping Tuff (~15–6 Ma)  
153 (Chen, 1997a; Song and Lo, 2002; Lai et al., 2017). A ~2 Myr time gap at the basal unconformity is  
154 characterized by an abrupt change in depositional age, cementation, clay mineralogy, and truncated normal  
155 faults that are restricted to the Tuluanshan Formation beneath the unconformity (Barrier and Angelier, 1986;  
156 Dorsey, 1992). Field and stratigraphic analysis for this study shows that the age gap is partly occupied by an  
157 eastward-younging thin discontinuous sequence comprised of the Biehchi Epiclastic Unit (~4 Ma), Kangkou  
158 Limestone (~5–3 Ma), and younger units of the Shihtiping Tuff (~4.2 Ma). (see details in *Section 6.1*)

159 The synorogenic Plio-Pleistocene succession of marine flysch and conglomerate in the Coastal Range  
160 records unroofing of metamorphic rocks in the Central Range orogen as documented with changes in  
161 abundance of metamorphic lithic fragments (e.g., Teng, 1979; Dorsey, 1985; Chen et al., 2019), illite  
162 crystallinity (Buchovecky and Lundberg, 1988; Dorsey et al., 1988; Yao et al., 1988), and reset detrital  
163 thermochronometers (Kirstein et al., 2009, 2014). Earlier stratigraphic studies named these deposits the  
164 Takangkou and Chimei formations (Hsu, 1956), or collectively the Takangkou Formation (e.g., Page and  
165 Suppe, 1981; Chang et al., 2000; Huang et al., 2008; Chen, W.-H. et al., 2015). Definitional problems and  
166 inconsistencies led to a newer nomenclature that subdivides the section into the Fanshuliao and Paliwan  
167 formations (Teng, 1987; Chen, 2009). The Fanshuliao Formation contains thick slumped and chaotic horizons  
168 in mudstone and fine-grained turbidites, with sand composed of volcanic lithic fragments, plagioclase feldspar,  
169 quartz sand, and carbonate bioclasts (Teng, 1980; Teng et al., 2002). The Paliwan Formation consists of thin-  
170 to thick-bedded turbidites and submarine conglomerates with abundant low-grade metamorphic lithic

171 fragments and only minor volcanic clasts (Teng, 1982; Chen, 1997a). The base of a widespread pebbly  
172 mudstone layer (Pm3) defines the contact between the Fanshuliao and Paliwan formations in the southern  
173 Coastal Range (Wang and Chen, 1993; Chen, 2009). Recent geologic mapping and stratigraphic analysis  
174 permits further subdivision based on recognition of multiple widespread marker beds of pebbly mudstone and  
175 tuffaceous turbidites (**Fig. 3**) (Lai and Teng, 2016; Lai, L.S.-H. et al., 2018).

176 The structure of the Coastal Range is dominated by large-displacement imbricate west-vergent thrust  
177 faults and associated regional-scale folds (Wang and Chen, 1993). Rapid uplift rates (e.g., Hsieh and Rau,  
178 2009; Chen et al., 2020), kinematic analyses (Barrier and Angelier, 1986; Lin et al., 1999), and modern  
179 seismicity (Angelier et al., 2000; Lee et al., 2006) provide evidence for ongoing active deformation and crustal  
180 thickening in the Coastal Range. Of the total Philippine Sea – Eurasian plate convergence rate (~82–90 mm  
181 yr<sup>-1</sup>), roughly 60 mm yr<sup>-1</sup> shortening is absorbed by convergence in the Coastal Range and offshore structures  
182 to the east (~60 km) in the past ~1 Myr (Reed et al., 1992; Tsai et al., 2015; Hsieh et al., 2020).

183 In the southern Coastal Range, several west-vergent thrust faults and three large plunging folds control  
184 the distribution of map units (**Fig. 4**) (Hsu, 1956; Wang and Chen, 1993; Lai and Teng, 2016). Among these  
185 structures, only the Longitudinal Valley fault is considered to be currently active (Angelier et al., 2000; Lee et  
186 al., 2006; Shyu et al., 2008). Most previous studies map the southern Tuluanshan fault along the drainage  
187 divide between the Taiyuan and Powhua regions (Wang and Chen, 1993; Chen, 1997b; Chang et al., 2000;  
188 Chen, W.-H. et al., 2017), but dipping depositional contacts and continuous stratigraphy suggest the absence  
189 of a major fault in that area (Barrier and Muller, 1984; Li, 1984; Lin et al., 2008). Field mapping for this study  
190 confirms the depositional nature of contacts where the southern Tuluanshan fault was originally proposed.  
191 West of there we have traced a ~100-300 m wide belt of 5-10 m wide fault zones with fault gouge and brittle  
192 shears aligned with the northern Tuluanshan fault, which we interpret as the southern Tuluanshan fault where  
193 it cuts the Chungye river (CYC) and the Mukeng river (MKC) sections. (see details in *Section 5*)

194



195 2.2. *Lichi Mélange*

196 The Lichi Mélange, originally named “Raikoka Formation” or “Lichi Formation” (Ooe, 1939; Hsu,  
197 1956), “consists mainly of poorly stratified mudstone in which some large or small rock fragments or blocks  
198 of hard greyish sandstone, gabbro, serpentinite, and a little slate are present” (Hsu, 1956). The mélange  
199 contains pervasive shear fabrics in poorly consolidated scaly mudstone and block-in-matrix textures (Chen,  
200 1997b; Chang et al., 2000; Chen, W.-H. et al., 2017; Huang et al., 2018). Other block lithologies include  
201 andesite, volcanoclastic rock, limestone, ophiolite-bearing sedimentary rocks, amphibolite, low-grade meta-  
202 sandstone, and flysch blocks similar to the Fanshuliao and Paliwan formations (Liou et al., 1977; Page and  
203 Suppe, 1981; Sung, 1991). Clay minerals in the matrix are illite with relatively abundant kaolinite, in contrast  
204 to illite- and chlorite-rich Fanshuliao and Paliwan formations, suggesting different sediment source rocks,  
205 routing systems, weathering conditions, or mixing processes (Lin and Chen, 1986). Depositional contacts and  
206 shear zones linked to soft-sediment deformation and post-depositional thrusting suggest a complex mixture of  
207 tectonic and sedimentary rock-mixing products (e.g., Page and Suppe, 1981; Chang et al., 2000).

208 Despite previously published evidence for both tectonic and sedimentary origins to the Lichi Mélange,  
209 two alternate hypotheses describe the primary mode of rock mixing as either tectonic or sedimentologic (Teng,  
210 1981; Chen, 1991; Huang et al., 2018) (**Fig. 2**). The currently prevailing hypothesis postulates that the Lichi  
211 Mélange formed by shearing of older forearc-basin sediments in a post-depositional mega-thrust zone (Chang  
212 et al., 2000, 2001; Huang et al., 2000, 2008, 2018; Chen, W.-H. et al., 2017), consistent with earlier models  
213 for deformation in a subduction-accretion complex (**Fig. 2A**) (e.g., Biq, 1977; Teng, 1981; Hsü, 1988; Chen,  
214 1991, 1997b). In this framework, zones with varying degree of stratal disruption and rock mixing  $\alpha$ - $\delta$  scheme  
215 of Raymond (1984) are all mapped as Lichi Mélange (Chang et al., 2000, 2001; Huang et al., 2008; Chen, W.-  
216 H. et al., 2017), and these mélange zones are defined as being bounded by discrete brittle thrust faults (Wang  
217 and Chen, 1993; Chen, 1997b). Thick segments of relatively coherent strata ( $\alpha$  and  $\beta$ ) are thus interpreted to  
218 be fault-bounded slivers of originally coherent sedimentary rocks, and exotic blocks (ophiolitic, volcanic,

219 volcanoclastic rock types) are considered to be tectonically emplaced structural fault slices (Huang et al., 2008,  
220 2018). Field observations reveal brittle scaly foliation and shear fabrics near the west-vergent Longitudinal  
221 Valley fault and Tuluanshan fault, particularly in the Powhua and Luye area (Chen, 1997b; Chang et al., 2000,  
222 2001). Foraminifera biostratigraphic data are proposed to support a depositional age of ~3.35 to 8.5 Ma for  
223 structurally disturbed strata in the Lichi Mélange, generally older than nearby exposures of the Fanshuliao and  
224 Paliwan formations (~ 4–1 Ma) (Huang et al., 2008, 2018; Chen, W.-H. et al., 2017). Unresolved challenges  
225 to this hypothesis include: (1) definition of mélange units that are based on genetic interpretations, making it  
226 difficult to assess the potential role of gravity-driven processes; (2) lack of consistent criteria for identifying  
227 tectonic faults; (3) contacts that were reported as depositional in original studies (Chang et al., 2000, 2001) or  
228 later work (Lin et al., 2008) remain unexplained; and (4) interpreted depositional ages of mélange matrix that  
229 are inconsistent with prior studies of calcareous nannoplankton biostratigraphy (see below).

230 A second group of studies interprets the Lichi Mélange as a complex of submarine-slide deposits  
231 derived from the steep fault-bounded western margin of the basin (e.g., Hsu, 1956; Wang, 1976; Ernst, 1977;  
232 Ho, 1977; Page and Suppe, 1981; Barrier and Muller, 1984). In this hypothesis, submarine slide blocks  
233 (olistoliths) are interbedded with and pass laterally into flysch facies of the Fanshuliao and Paliwan formations,  
234 and were later overprinted (tectonically reworked) by post-depositional brittle tectonic faults. This multi-stage  
235 hypothesis is supported by analogue modeling (e.g., Malavieille et al., 2016, 2021) and seismic reflection  
236 studies of offshore chaotic bodies in the North Luzon Trough that are proposed as a modern equivalent of the  
237 Lichi Mélange (e.g., Huang et al., 1997; Chi et al., 2014). Within this framework, the Lichi Mélange, or “Lichi  
238 Formation” (Hsu, 1956), was originally defined as chaotic disrupted broken formation and mixed block-in-  
239 matrix rocks (mélange) with locally interbedded coherent layers of conglomerate, pebbly mudstone, slump  
240 beds, mudstone, and flysch (Liou et al., 1977). Few undisputed depositional contacts have been reported  
241 between mélange and coherent strata associated with soft-sediment stretching, bending, folding, or  
242 fragmentation of blocks (Page and Suppe, 1981; Li, 1984). Early studies showed that calcareous nannoplankton

243 assemblages in Lichi Mélange matrix are similar to those of nearby Plio-Pleistocene Fanshuliao and Paliwan  
244 formations (< ~4 Ma), and that exotic sedimentary blocks yield older fossils (~18 to 5.6 Ma) consistent with  
245 an olistostromal interpretation (Chi et al., 1981; Barrier and Muller, 1984; Li, 1984).

246 However, the sedimentary hypothesis also faces challenges: (1) coherent portions of the “Lichi  
247 Formation” are similar to the Fanshuliao and Paliwan formations, creating ambiguities in the definition of  
248 stratigraphic units and boundaries; (2) few depositional contacts have been reported in prior published studies;  
249 (3) distal olistostromal facies that are predicted by this hypothesis have not previously been identified in nearby  
250 Fanshuliao and Paliwan formations to the east (Teng, 1981; Chen, 1991); and (4) because Miocene sedimentary  
251 rocks were not recognized in the eastern part of the Central Range directly to the west, some workers argued  
252 there is no source area to supply Miocene-age sedimentary slide blocks and olistoliths (Huang et al., 2018).

253 Taken together, inconsistent stratigraphic definitions and age interpretations have led to major  
254 disagreements over the distribution, contact relationships, and origins of the Lichi Mélange. Recent studies of  
255 mélange-like marker beds (pebbly mudstone) in the Fanshuliao and Paliwan formations (Lai and Teng, 2016;  
256 Lai, L.S.-H. et al., 2018), and a late Miocene depositional age for metasedimentary rocks in the eastern part of  
257 the Central Range (e.g., Chen, W.-S. et al., 2017; Mesalles et al., 2020), have not yet been considered in this  
258 debate. These new findings reveal a need to re-evaluate critical field relationships in the Lichi Mélange, refine  
259 its definition, and reassess its stratigraphic context in the southern Coastal Range (**Fig. 1B**).

260

### 261 *2.3 Nomenclature and definitions used in this paper*

262 In this study, we adopt modern nongenetic terms of “mélange” and “broken formation” to describe  
263 mappable (at 1:25,000 or smaller scale) chaotic rocks that commonly have “pervasively deformed and  
264 fragmented matrix of finer-grained material”, with and without inclusion of extra-formational blocks  
265 respectively (Hsü, 1968; Silver and Beutner, 1980; Raymond, 1984), which represent products of different  
266 forming mechanisms – rock-mixing plus stratal disruption versus only stratal disruption (Harris et al., 1998;

267 Festa et al., 2012). The terms “olistostrome” and “olistolith”, traditionally equivalent to “sedimentary mélangé”  
268 and “slide blocks” following classic principles of stratigraphic superposition (Abbate et al., 1970), are applied  
269 to name sedimentary lithofacies in the Lichi Mélangé (**Table 1**). The term “polygenetic mélangé” is used for  
270 a mélangé body formed through a multistage evolution that involves two or more styles of rock-mixing  
271 mechanisms (sedimentary, tectonic, or diapiric), and its primary fabrics have been overprinted (reworked) by  
272 later processes (Berkland et al., 1972; Ogata et al., 2019b; Festa et al., 2020).

273 For the stratigraphic framework, this paper adopts an updated descriptive nomenclature and  
274 depositional ages for lithostratigraphic units in the Coastal Range, summarized in **Fig. 3**. The Tuluanshan  
275 Formation (Chen, 1997a; Song and Lo, 2002) is capped by a regional unconformity (Dorsey, 1992) and is  
276 overlain by 4-7 km of marine flysch of the Fanshuliao and Paliwan formations (Teng, 1987; Chen, 2009; Lai  
277 and Teng, 2016; Lai, L.S.-H. et al., 2018). Due to the difficulty of defining the contact between the Lichi  
278 Mélangé and flysch units, we classify the products of sedimentary processes (i.e., lithofacies) independent of  
279 any existing lithostratigraphic classification scheme (**Table 1**, see details in *Section 4*). The Lichi Mélangé in  
280 this study is defined narrowly as rocks (facies X3, olistostrome) characterized by poorly developed  
281 stratification that is broadly parallel to regional bedding (equivalent to the “color bands” in Page and Suppe,  
282 1981) and pervasively “sheared” matrix with extra-formational blocks (i.e., scaly block-in-matrix fabric).  
283 Chaotic sedimentary rocks without internal shear fabric or foliation that record soft-sediment deformation and  
284 sediment gravity flows (i.e., pebbly mudstones (facies X1), slump beds (facies X2), and other coherent strata  
285 (facies F1-F4, Vo)) are included in the Fanshuliao and Paliwan formations. For outsized (>10 m to a few km  
286 diameter) fractured blocks regardless of lithology that appear in all sedimentary units, we apply the neutral  
287 term “olistolith” (facies X4).

288 The term “exotic block” is reserved for blocks with lithologies whose source is not present in the  
289 surrounding sedimentary units (e.g., andesite, volcanoclastic sandstone and conglomerate, limestone), and  
290 which are different from any lithology found in country rocks of the Coastal Range (e.g., well-lithified quartz-

291 rich sandstone without orogen-derived lithic fragments, ophiolitic rocks (gabbro, serpentinite, granodiorite,  
292 etc.), metasandstone) (Liou et al., 1977; Page and Suppe, 1981), in contrast to some blocks originated from  
293 nearby intra-formational sources such as turbidite facies F2 (so called “native blocks”).

294 It should be noted that the definition of Lichi Mélange as a lithostratigraphic unit in this study is used  
295 in a manner of convenience for assessing the geologic map pattern and observed contact relationships, thus  
296 serving as the basis for additional analyses, which is different from the classic usage of the lithological term  
297 “mélange.” Some chaotic facies in the Fanshuliao and Paliwan formations such as pebbly mudstone (X1) and  
298 part of slump bed (X2) can be also considered as “sedimentary mélange (olistostrome)” as conventionally  
299 defined (Ogata et al., 2019b) or “small-scale mélanges and broken formations” if they are not mappable at  
300 1:25,000 or smaller scale (e.g., Codegone et al., 2012).

301

### 302 **3. Methods**

303 Detailed geological mapping for this study targeted the Lichi Mélange and associated deposits exposed  
304 in road cuts and riverbanks of the southern Coastal Range (**Fig. 4**). Lithostratigraphic descriptions were  
305 executed in selected river sections along three geological transects: (1) Powhua-Shinchang; (2) Luye-Tulan;  
306 and (3) Fuli-Chengkung transects (**Figs. S1-S14**). Among these sections, we compiled existing data for  
307 microfossil biostratigraphy and magnetostratigraphy from previous studies (Chang, 1967, 1969; Barrier and  
308 Muller, 1984; Chen, 1988b; Huang and Yuan, 1994; Horng and Shea, 1996; Chen, W.-H. et al., 2015, 2017)  
309 and manually georeferenced their sample localities on maps in order to project them to our measured sections  
310 (**Figs, S3-S9**). We also include digitized unpublished calcareous nannoplankton fossil data from Chi et al.  
311 (1981) in our analysis (**Fig. 3** and **Table S3**). We also collected fresh mud rock samples for new microfossil  
312 analysis in the Lichi Mélange matrix and surrounding sedimentary units from all studied river sections (**Figs.**  
313 **S3-S9**), with a focus on calcareous nannoplankton data that were relatively limited in previous studies and  
314 three additional samples for planktonic foraminifera identifications (the Yungfong (YF) section) (**Tables S3-**

315 **S4**). Additional paleomagnetic drill core samples were collected from strata in coherent continuous sections  
316 (Fanshuliao and Paliwan formations), and processed through stepwise thermal demagnetization, alternating-  
317 field demagnetization, or a combination of both methods to obtain reliable measurements of primary remanent  
318 component of the paleomagnetic declination and inclination at each site (**Fig. S17**). A “double-tilt correction”  
319 was later applied to progressively remove tilting by regional fold plunge and then bedding tilt (Fisher, 1953;  
320 Ramsay, 1961) (**Table S5**). After compiling these magneto-biostratigraphy datasets, we interpreted the  
321 depositional ages based primarily on paleomagnetic polarity reversals and the first appearance datum (FAD)  
322 for index fossils due to potential fossil reworking (Chi et al., 1981; Chen, 1988b, 2009), whose ages follow  
323 recent compilations for the Indo-Pacific region (Anthonissen and Ogg, 2012; Backman et al., 2012; Ogg, 2012;  
324 Chuang et al., 2018) (**Fig. 3**).

325 To understand paleo-basin geometry and facies architecture, we constructed three stratigraphic panels  
326 by correlating stratigraphic sections along W-E transects (Powhua-Shinchang, Luye-Tulan, Fuli-Chengkung)  
327 and hanging the youngest widespread chronostratigraphic horizons, or datums, such as the first appearance  
328 datum (FAD) of microfossils, paleomagnetic reversals, and event marker beds like pebbly mudstone (X1) and  
329 tuffaceous turbidites (Vo). The approximate unfolded horizontal distance was calculated using standard  
330 geometrical methods (e.g., Ragan, 2009) and mean bedding dip along the transects (**Fig. 4**).

331 To reconstruct sediment routing pathways and sediment sources, we measured sedimentary structures  
332 for paleocurrent (e.g., flute casts, ripple cross-lamination, imbricated gravel clasts) and paleoslope (e.g., axial  
333 planes of asymmetric slump folds) directions in each studied section and the Loho and Changpin areas,  
334 including data for tuffaceous turbidites (Lai, L.S.-H. et al., 2018). All directional data were restored to paleo-  
335 horizontal using a “double-tilt correction”. More comprehensive descriptions of our methodologies are  
336 included in the *Supplementary Materials*.

337

#### 338 **4. Lithofacies and facies associations**



339           Nine lithofacies are identified in Plio-Pleistocene sedimentary rocks of the southern Coastal Range  
340 based on their distinctive characteristics and corresponding interpreted sedimentary processes (**Table 1**). We  
341 employ the classification scheme of Raymond (1984), in which categories  $\alpha$  to  $\delta$  are used to indicate degree  
342 of stratal disruption. This scheme was widely applied in previous studies of the Lichi Mélange (e.g., Chang et  
343 al., 2001; Chen, W.-H. et al., 2017). Lithofacies are then grouped into three facies associations according to  
344 their stratigraphic context, sedimentological affiliations, and contact relationships, and these are used to  
345 interpret depositional processes, paleoenvironments, and other rock-forming mechanisms (**Table 2**).

346           Facies Association 1 (FA1) consists of submarine flysch deposits spanning a wide range of grain size  
347 and sedimentary features comprising most of the Fanshuliao and Paliwan formations. The major facies in this  
348 group are mudstone (facies F1), turbidites (F2), thick-bedded sandstone and gritstone (F3), and conglomerate  
349 (F4) (**Fig. 5A, B, C**). Finer-grained facies in this association are the depositional products of cohesionless  
350 sediment gravity flows including sand-rich low- to high-density turbidity currents and gravel-rich grain flows  
351 (**Table 1**). Clasts in this facies association are primarily composed of orogen-derived lithic fragments (e.g.,  
352 slate, low-grade metasandstone), followed by minor andesite and mafic rocks (e.g., basalt, gabbro). They are  
353 interpreted as the deposits of proximal to outer submarine fans with supra-fan lobes and channels that formed  
354 on a deep basin plain (Chen, 1988a; Dorsey and Lundberg, 1988). The deep-sea fan deposits likely were  
355 derived from submarine canyons that funneled sediment downslope from onshore river sources (Stow and  
356 Mayall, 2000).

357           Facies Association 2 (FA2) includes sedimentary deposits that display a wide range of chaotic textures  
358 and internal structures formed by stratal disruption, slumping, sliding, and/or rock-mixing (**Table 2**).  
359 Extraformational clasts (pebble size and larger) in these facies include meta-sandstone, slate, volcanic andesite,  
360 volcanoclastic rocks, ophiolitic rocks (gabbro, serpentinite, granodiorite), limestone, and well-sorted quartz-  
361 rich sandstone (Liou et al., 1977; Page and Suppe, 1981; Chen et al., 2008; Lai, L.S.-H. et al., 2018). Pebbly  
362 mudstone (X1) and slump beds (X2) represent ductilely deformed and disrupted sediments in the Fanshuliao

363 and Paliwan formations (**Fig. 5E, F**). These facies locally include outsized, decimeter- to kilometer-scale  
364 olistoliths (X4) (**Fig. 6A, B**) that commonly display small-scale internal brittle fractures and local diapiric  
365 mudstone intrusions (**Fig. 7C**) indicating rapid emplacement in unconsolidated sediment that created local  
366 fluid overpressure (Ogata et al., 2019a). These olistoliths are composed of various extra-formational lithologies  
367 such as andesite, volcanoclastic sandstone and conglomerate, ophiolitic rocks (gabbro, serpentinite,  
368 granodiorite, etc.), limestone, and quartz-rich sandstone (**Figs. 6A-E, S1-S12**). Olistostrome facies (X3) are  
369 characterized by very thick massive beds of disturbed mudstone with indistinct bedding and relatively weak  
370 shear fabrics (**Fig. 6D-E**). Intensive rock dismemberment including characteristic boudinage structures occurs  
371 locally within the basal zone of slump beds facies (X2) (**Fig. 6F**), fitting the definition of “broken formation.”  
372 Well-developed scaly foliations with connective tightly spaced slickensides, schistosity-cisaillement (S-C)  
373 fabrics, and reoriented clasts with extensional structures commonly occur along sheared horizons near the base  
374 of the olistostrome (X3) (**Figs. 6G, S15B**). These basal deformation features in chaotic sedimentary rocks may  
375 be the result of gravitational-related shearing during mass movements (Tripsanas et al., 2008; Ogata et al.,  
376 2014). Detailed field observations reveal depositional successions of chaotic facies (FA2) interpreted as  
377 products of submarine mass wasting and flow transformations from slides and slumps to cohesive debris flows  
378 that initiated on mud-rich unstable submarine slopes and accumulated at base-of-slope to proximal basin plain  
379 environments (Ogata et al., 2012; Festa et al., 2016) (**Table 2**).

380 Lastly, FA3 consists of tuffaceous turbidites (Vo) (**Fig. 5D**) that represent distal syn-eruptive  
381 volcanoclastic deposits associated with syn-collision volcanism of the Luzon Arc (Yang et al., 1995; Lai, L.S.-  
382 H. et al., 2018).

383 This classification scheme permits interpretation of processes using a modern evidence-based  
384 approach that provides an unambiguous basis for defining lithostratigraphic units (**Tables 1, 2**). The Lichi  
385 Mélange in this scheme is restricted to facies that display pervasive shear fabrics: olistostrome (X3) (**Fig. 6D,**  
386 **E**). In contrast, coherent facies (F1-F4), and mixed facies produced by sediment gravity flows and slumping



387 (X1, X2) are assigned to the Fanshuliao and Paliwan formations (**Fig. 5**). Olistoliths (X4) are included in the  
388 lithostratigraphic unit of its surrounding facies (**Fig. 6A, B, C**).

389

## 390 **5. Contact and map relationships**

391 In our field survey, we first identified the fault zone rocks (i.e., uncompact cataclasite, fragmented  
392 mudstone with pencil cleavage, and fault gouge) of the Tuluanshan fault (**Fig. 7**), which cuts all lithological  
393 units including Lichi Mélange in the southern Coastal Range (**Figs. 4, S1-S2**). These fault zone rocks display  
394 brittle shear fabrics with well-polished slickensides that overprint primary sedimentary fabrics and structures  
395 of rocks on both sides of the main fault. This observation confirms that brittle shear fabrics are not diagnostic  
396 for differentiating chaotic rocks generated by different mechanisms (cf. Chen, 1997b; Chang et al., 2000),  
397 and the “structurally ordered block-in-matrix fabrics” subject to tectonic overprints are restricted to narrow  
398 fault-damage zones.

399 In contrast to identified brittle fault contacts, most contacts between Lichi Mélange and other  
400 sedimentary units are depositional. Eight of the best exposed depositional contacts are documented in **Fig. 8**,  
401 including the classic outcrops reported by Page and Suppe (1981) (their Locality J) (**Fig. 8A**) and Li (1984)  
402 (their site L12) (**Fig. 8C**). According to stratigraphic younging direction indicated by sharp bases and normally  
403 graded Bouma sequences in turbidites (facies F2), the Lichi Mélange is both underlain and overlain by deposits  
404 of the Fanshuliao and Paliwan formations, in exposures that reveal clear interbedding relationships.  
405 Depositional contacts in Chungye river – A (CYCa) and Yungfong (YF) sections exhibit gradational transitions  
406 from deposits of non-cohesive sediment gravity flows (facies association FA1) to submarine mass-wasting  
407 products (FA2), thus displaying clear conformable lithological transitions that reflect straightforward  
408 depositional contact relationships (**Figs. 10, S15-S16**).

409 The degree of shearing at depositional contacts varies from none (e.g., **Fig. 8A, B, D, H**) to high (e.g.,  
410 **Fig. 8F**). None of the sheared contacts coincides with post-diagenetic brittle fault gauge, cataclasite, or pencil

411 cleavage, making them easily distinguished from brittle fault zones of the Tuluanshan fault (**Fig. 7**) and  
412 Wushinshih fault (Lai and Teng, 2016). There is no evidence of shearing at the depositional contacts between  
413 Lichi Mélange and Fanshuliao Formation near the headwaters of Mukeng river (MKC) section (**Figs. 4, 8C,**  
414 **D, S2**), which previous workers speculated is the southern extent of the Tuluanshan fault (e.g., Chen, 1997b;  
415 Chang et al., 2000; Huang et al., 2018). Similarly, the well exposed depositional contact at Chunchie river  
416 (CC), Chiaolai river (CLC), and Juchiang river (JCC) sections around Fukang area (Page and Suppe, 1981;  
417 Lin et al., 2008) clearly refute a previously hypothesized east-vergent thrust at that locality (e.g., Chang et al.,  
418 2001; Chen, W.-H. et al., 2017; Huang et al., 2018) (**Fig. 8A**).

419         Some studies map a “Yungfong fault” at the contact between Lichi Mélange and Fanshuliao  
420 Formation in the Yungfong (YF) section (**Figs. 4, S2**), with variously proposed vergence directions (west-  
421 vergent *or* east-vergent) (Lo et al., 1993; Chen, 1997b; Chang et al., 2000). Soft-sediment extension features  
422 (boudinage) are commonly observed in the Lichi Mélange (i.e., olistostrome (X3)). Scaly foliation near the  
423 basal sheared contact has an attitude identical to regional bedding dipping toward west (**Fig. 8G**), and it  
424 correlates laterally to another exposure 0.6 km to the north where an unambiguous depositional contact is  
425 reported (Hsu, 1956; Barrier and Muller, 1984) (**Figs. 8H, S16**). The sense of shear measured along this  
426 localized sheared horizon seems to be consistent with the orientation of regional tectonic stress field (Chen,  
427 1997b; Chang et al., 2000), but is also consistent with reconstructed paleoslope directions after bedding  
428 corrections, suggesting an alternative explanation of gravity-driven sliding and basal shear (see *Section 7.1*).  
429 These relations suggest that localized shear fabrics near the southern contact represent localized shears  
430 produced by mass movement at the base of thick olistostrome beds. The YF section appears to be a continuous  
431 succession, an interpretation supported by internal consistency among index microfossils (see *Section 6.1*).

432         Based on careful assessment of contact relationships, our geological map reveals common pinch-out  
433 of the Lichi Mélange with lateral and vertical facies transitions to pebbly mudstone beds (X1) of the Fanshuliao  
434 and Paliwan formations (**Figs. 4, S1-S2**), thus confirming their interbedding relationship. The Lichi Mélange

435 is primarily preserved in the western part of the Coastal Range, except in the Fukang area where thick Lichi  
436 Mélange extends to the east and southeast where it is exposed along the modern coastline (**Fig. 4**). The internal  
437 stratification and shear fabrics of the Lichi Mélange broadly coincide with regional bedding trends (Page and  
438 Suppe, 1981). We also observe random fabric orientation, particularly around Fukang area, and locally  
439 preserved onlap onto channel margins (**Fig. 8E**), revealing a map pattern typical of large-scale sedimentary  
440 mélangé (Festa et al., 2019). Lichi Mélange and other units in this area were reworked together by post-  
441 depositional tectonic deformation (cross-cutting thrust faults and folds) (**Figs. 4, 7**), and therefore the Lichi  
442 Mélange can be considered as a “polygenetic mélangé.”

443

## 444 **6. Basin-fill stratigraphy of the southern Coastal Range**

### 445 *6.1 Age of sedimentary units and unconformities in the southern Coastal Range*

446 The sedimentary fill of the southern Coastal Range basin is dominated by Plio-Pleistocene deep-  
447 marine orogen-derived deposits that formed by gravity-driven processes (Lichi Mélange, Fanshuliao and  
448 Paliwan formations). These deposits overlie an eastward younging regional unconformity on top of Miocene  
449 Shihmen Volcanic Breccia and older Shihtiping Tuff of the Tuluanshan Formation (**Fig. 3**).

450 Our compilation of age data shows that the same group of youngest index microfossils are present in  
451 the matrix of Lichi Mélange and interbedded Fanshuliao and Paliwan formations (**Figs. 9, 10, S3-S14**).  
452 Microfossils whose last-appearance ages are older than the first appearance datum (FAD) of younger ones  
453 repeatedly appear in both Lichi Mélange and interbedded units, indicating persistent fossil reworking that  
454 limits the reliability of the Last Appearance Datum (LAD) for interpretations of depositional age. Planktonic  
455 foraminifera *Globorotalia crassaformis* (FAD 4.31 Ma), *Globorotalia tosaensis* (FAD 3.35 Ma) and  
456 calcareous nannoplankton *Pseudoemiliania lacunosa* (FAD 3.82 Ma) are present in the oldest strata which are  
457 exposed in the west, including Mukeng river (MKC), Chungye river (CYC), and Yungfong (YF) sections  
458 (Chang, 1967; Barrier and Muller, 1984; Chen, W.-H. et al., 2017) (**Figs. 10, S3-S7, S11-S13**). At the southeast

459 end of the Coastal Range (Fukang area) (**Figs. 4, S1**), calcareous nannoplankton *P. lacunosa* (FAD 3.82 Ma)  
460 and trace *Gephyrocapsa oceanica* (FAD 1.70 Ma) are present in Lichi Mélange in the Chunchie (CC), Chiaolai  
461 river (CLC), and Moon World (MW) sections (Chi et al., 1981; Chen, W.-H. et al., 2017). Large *Gephyrocapsa*  
462 spp. (FAD 1.57 Ma) appears near the top of the underlying Paliwan Formation (**Figs. 10C, 11, S5-S6, S12**).  
463 Although older (Miocene) calcareous nannoplanktons *Reticulofenestra pseudoumbilicus* (medium and large),  
464 *Sphenolithus abies*, and *Discoaster* spp. are abundant in the matrix of the Lichi Mélange in this area, the clear  
465 evidence for an unsheared depositional contact with stratigraphic superposition (**Fig. 8A**) and common  
466 olistostromal features (**Fig. 6D**) indicate that the Miocene fossils are reworked from older sediments (**Fig. 11**).  
467 Thus, the whole sedimentary sequence in the southern Coastal Range was deposited between ca. 4 and 1 Ma,  
468 and the depositional age of the Lichi Mélange is similar to that of interbedded Fanshuliao and Paliwan  
469 formations.

470           The Kangkou Limestone is only preserved at the base of the Sanshian river (SSS), Shingang river  
471 (SGS), and Babian river (BBS) sections (**Figs. 4, S8, S9**). In this area, it contains planktonic foraminifera *Gr.*  
472 *crassaformis* (FAD 4.31 Ma) at the base and abundant *Gr. tosaensis* (FAD 3.35 Ma) and *Dentoglobigerina*  
473 *altispira* (LAD 3.05 Ma) near the top (**Fig. S14**), suggestive of a depositional age range between 4.31 and 3.05  
474 Ma (Huang and Yuan, 1994). Huang and Yuan (1994) interpreted that the top of the Kangkou Limestone may  
475 be younger based on a single, uncertainly identified specimen of *Globorotalia truncatulinoides* (FAD 2.00 Ma)  
476 (Sample #26 in their Table 4). This tentative age assignment is not considered in our compilation because it  
477 could not be verified. The Biehchi Epiclastic Unit is exposed at the base of the Bieh river (BC) section and  
478 was deposited at ca. 4.2–3.8 Ma based on the presence of planktonic foraminifera *Gr. crassaformis* (FAD 4.31  
479 Ma) (Chang, 1969), calcareous nannoplankton *P. lacunosa* (FAD 3.82 Ma) (Barrier and Muller, 1984), and  
480 the youngest peak U-Pb age (~4.2 Ma) of detrital zircon (Chen, T.-W. et al., 2015). The age distribution of  
481 these two intermittent units partially overlaps that of the Lichi Mélange and lower Fanshuliao Formation, and

482 appears to be a discontinuous record of the ~2 Myr transition from the youngest stages of arc volcanism to  
483 sedimentary basin formation during collisional orogenesis (Dorsey, 1992).

484

#### 485 6.2 Type sections and marker beds of the Fanshuliao and Paliwan formations

486 The Madagida river (MDJ) and Bieh river – A (BCa) sections are widely accepted as stratotypes for  
487 the Fanshuliao and Paliwan formations in the southern Coastal Range (Chen, 2009; Huang et al., 2018) (**Fig.**  
488 **9**). Widespread layers of pebbly mudstone (Pm1 to Pm7, facies X1) and tuffaceous turbidites (Tp1 to Tp14,  
489 facies Vo) provide useful marker beds that allow us to map and correlate these deposits (Lai and Teng, 2016;  
490 Lai, L.S.-H. et al., 2018). In this study, we discovered five more tuffaceous turbidites (Tf1 to Tf5) in the  
491 Fanshuliao Formation (**Fig. 3**). The Paliwan Formation in the MDJ section was previously dated between ca.  
492 2.15 to 1.5 Ma (Horng and Shea, 1996). In this study we refine the age interpretation with revised placement  
493 of the first occurrences of *G. oceanica* (FAD 1.70 Ma) and large *Gephyrocapsa* spp. (FAD 1.57 Ma) in this  
494 section (**Fig. 9A**). The proposed age of the Fanshuliao Formation in the southern Coastal Range varies from ~  
495 4.94–3.35 Ma (Lee and Chi, 1990; Chen, 2009) to ~ 3.35–2.15 Ma (Horng and Shea, 1996; Lai and Teng,  
496 2016). Based on compilation of previous and new data with lithostratigraphic correlations, the lower  
497 Fanshuliao Formation is reassigned here to the upper Gauss Chron, ranging in age from the top of the Keana  
498 reverse polarity event (C2An.1r; 3.04 Ma) to the Gauss-Matuyama boundary at 2.59 Ma. The upper Fanshuliao  
499 Formation corresponds to the lower Matuyama Chron (C2r.2r, 2.59–2.14 Ma) (**Fig. 9B**). This revised age  
500 interpretation is supported by the presence of planktonic foraminifera *Gr. tosaensis* (FAD 3.35 Ma) near the  
501 bottom of the section (site 222 in Chang, 1969) (**Figs. S7, S13B**).

502 Pebbly mudstone and tuffaceous turbidite marker beds have unique sedimentary textures and clast  
503 compositions that permit regional correlation. These marker beds are interpreted to record distinct geological  
504 events such as seismicity-triggered submarine debris flows and volcanic eruptions (Chen et al., 2008; Lai, L.S.-  
505 H. et al., 2018). This allows us to tune their ages using our updated high-resolution magneto-biostratigraphy,

506 and we use the marker beds as age anchors for other sections based on detailed geologic mapping and  
507 lithostratigraphic correlation. For example, pebbly mudstone beds Pm2, Pm3, and Pm5 were deposited near  
508 the Gauss-Matuyama boundary (2.59 Ma), the onset of *Pulleniatina* spp. left coiling event 5 (2.15 Ma), and  
509 the top of the Olduvai normal polarity event (C2n, 1.80 Ma), respectively. Tuffaceous turbidites Tp7-Tp14  
510 formed between the FAD of large *Gephyrocapsa* spp. (1.57 Ma) and onset of small *Gephyrocapsa* spp. acme  
511 zone (1.23 Ma), consistent with ages determined by apatite fission tracks ( $1.5 \pm 0.1$  Ma) and U-Pb zircon dating  
512 ( $1.6 \pm 0.1$  Ma) on equivalent beds (Yang et al., 1995; Chen, T.-W. et al., 2015). The tuffaceous turbidites Tp3-  
513 Tp4 and pebbly mudstone Pm4 formed around the base of the Olduvai event ( $\sim 1.95$  Ma), and the tuffaceous  
514 turbidites Tf1-Tf2 and pebbly mudstone Pm1 form near the base of C2An.1n event in Gauss Chron ( $\sim 3.04$   
515 Ma).

516

### 517 *6.3 Stratal architecture of the southern Coastal Range*

518 Using correlations summarized above and restored distances between stratigraphic sections, we  
519 constructed 2D west-east facies panels that reveal the original paleo-basin geometry along three studied  
520 stratigraphic transects (**Figs. 12, 13**). The panels show that sedimentary strata of the Fanshuliao and Paliwan  
521 formations and Lichi Mélange onlap onto a basin-wide basal unconformity on top of the Tuluanshan Formation  
522 (arc volcanic basement). The basal unconformity has a restored gentle west dip ( $\leq 6 - 7^\circ$ ) and defines an  
523 asymmetric basin low that corresponds to maximum stratigraphic thicknesses near the orogenic front (Dorsey,  
524 1992; Chen, 2009). All members of the Fanshuliao and Paliwan formations thin consistently to the east.

525 The reconstructed stratigraphic architecture of eastward thinning and onlap in Plio-Pleistocene orogen-  
526 derived deposits of the southern Coastal Range is unlike the arc-ward thickening stratal pattern that is typically  
527 observed in forearc basins (Noda, 2016, 2018). The observations of paleo-basin geometry and evidence for  
528 considerable basal erosion are inconsistent with previous interpretations that the Coastal Range deposits  
529 represent the sedimentary fill of an inherited, uneroded forearc basin (cf. Teng et al., 1988; Chang et al., 2000).

530 There is no evidence for a large local bathymetric low to support a backarc basin interpretation (cf. Chen,  
531 1988a, 1997a; Song and Lo, 2002) or pull-apart intra-arc basin (cf. Huang et al., 1995, 2006; Chen, W.-H. et  
532 al., 2015). Instead, the stratal pattern is best explained as the basin fill of a flexural foredeep basin where  
533 deposits thicken toward the orogen that supplied sediment to the basin (DeCelles and Giles, 1996; Sinclair and  
534 Naylor, 2012). This interpretation is consistent with the predictions of a syn-collisional retrowedge basin model  
535 proposed in other studies (e.g., Dorsey and Lundberg, 1988; Lundberg and Dorsey, 1988; Malavieille et al.,  
536 2016; Chen et al., 2019). (See details in *Section 8.2*)

537

## 538 **7. Paleoslope and paleocurrent data**

### 539 *7.1 Paleoslope orientations*

540 Paleoslopes determined from vergence direction of asymmetric slump folds (facies X2) show  
541 prevailing east to southeast slump directions in modern coordinates (**Fig. 14A**). Our results are consistent with  
542 previously published data in the Luye region (Page and Suppe, 1981) that indicate a regional east to southeast-  
543 dipping paleoslope in the southern Coastal Range. Structural and bedding-corrected striae measured at the  
544 basal depositional contact of Lichi Mélange in YF section (site #5-6 in figure 7 of Chang et al., 2000) (**Fig.**  
545 **8G**) and base of a thick exotic sandstone block in JCC section (site #1-2 in figure 8 of Chang et al., 2001)  
546 (**Figs. S5, S12B**) indicate shear directions consistent with local paleoslope indicators, suggesting that they  
547 originated by the similar mass-wasting processes (**Fig. 14A**). After correcting for  $30^{\circ}\pm 10^{\circ}$  clockwise block  
548 rotation based on paleomagnetic fabrics (Lee et al., 1990), our results imply a north-striking, east-dipping steep  
549 slope at the tectonically controlled western basin margin. This slope was the site of common submarine mass  
550 wasting events that generated the Lichi Mélange and associated submarine debris flows (Page and Suppe, 1981;  
551 Dorsey and Lundberg, 1988). Minor westward paleoslope directions near the base of the BCa section are  
552 interpreted to represent local structural complexities, and do not record a regional-scale west-dipping slope on  
553 the western flank of a volcanic arc massif (cf. Huang et al., 1995; Chen, 1997a; Song and Lo, 2002).

554

555 *7.2 Paleocurrent directions*

556 Paleocurrent directions exhibit temporal and spatial variations among different lithofacies (**Fig. 14B**).  
557 In orogen-derived turbidites and other cohesionless sediment gravity flow facies (F2-F4), paleotransport is  
558 dominantly toward the south in modern coordinates, with increasing indicators of southeastward transport in  
559 the southern region. We observe an up-section increase of southeast- transport directions in the younger  
560 Paliwan Formation, which is mainly preserved in the eastern part of the basin. Pebbly mudstone (facies X1)  
561 shows a dominant paleocurrent toward the southeast (in modern coordinates), consistent with paleoslope  
562 directions measured in slump bed (facies X2) nearby (**Fig. 14A**). In contrast, tuffaceous turbidites (facies Vo)  
563 have diverse paleocurrent directions with a relatively stronger components of westward to southwestward  
564 paleoflow directions.

565 After correcting for  $30^{\circ}\pm 10^{\circ}$  clockwise block rotation in the Coastal Range rocks (Lee et al., 1990),  
566 we use paleoslope and paleo transport indicators to interpret the location of source areas and sediment-routing  
567 pathways for each facies association. The main source of facies association FA1 (facies F2-F4), which formed  
568 in a submarine fan system (**Table 2**), was located northwest of the basin (Teng, 1982; Chen, 1997a). The up-  
569 section increase in east-directed paleocurrents implies increased input from the west, which we interpret as a  
570 response to eastward migration and basinward advance of the Taiwan collisional orogenic front. Consistent  
571 east- to southeast-directed directions of paleocurrent in FA1 and paleoslope in pebbly mudstone (X1) and  
572 slump beds (X2) reveal a north-trending, east-dipping submarine slope at the steep unstable western basin  
573 margin. This shows that the eastern retrowedge of the Taiwan orogen was the main source of mass-transport  
574 deposits in facies association FA2. Syn-eruptive tuffaceous turbidites (FA4) display spatially variable  
575 paleocurrent directions with a dominant mode to the west and southwest (**Fig. 14B**). These turbidites were  
576 derived from an active volcanic source east of the basin, not the volcanic island of Lutao located southeast of  
577 the modern Coastal Range (cf. Yang et al., 1995; Horng and Shea, 1996) (**Fig. 1**). Our interpretation of an



578 eastern source is supported by a westward decrease in thickness of the tuffaceous turbidites (Lai, L.S.-H. et al.,  
579 2018).

580

## 581 **8. Discussion**

### 582 *8.1 Paleogeography and depositional setting*

583 Stratigraphic panels in the southern Coastal Range reveal an important pattern of lateral facies change  
584 in which western sections contain abundant olistostromal facies (association FA2), and age-equivalent sections  
585 in the east are dominated by flysch facies (association FA1) (**Figs. 12, 13**). Proximal facies including slump  
586 beds (X2), olistostromes (X3), and olistoliths (X4) are more abundant in the west and pass laterally into distal  
587 facies with pebbly mudstone beds (X1) in the east. This facies architecture records downslope disintegration  
588 of mass flows during transformation from slides, slumps, and blocky flows to cohesive debris flows to high-  
589 density turbidity currents (Nemec, 1990; Ogata et al., 2012; Festa et al., 2016) (**Fig. 15B**), consistent with  
590 measured dominant eastward paleoslope directions (**Fig. 14A**). These facies associations formed by submarine  
591 slumping and deposition by sediment gravity flows in deep-water slope to submarine fan and basin plain  
592 environments (**Fig. 15A**). The depositional setting was subject to frequent deliveries of orogen-derived  
593 sediment that was routed into the basin by a combination of widespread slope failures and gravity-driven  
594 transport funneled through submarine canyons (Stow and Mayall, 2000).

595 Minor syn-eruptive tuffaceous turbidites (facies Vo, association FA4) represent a distal record of arc  
596 volcanism during ~4–1 Ma deposition of the orogen-derived sedimentary sequence (Lai, Y.-M. et al., 2018;  
597 Song and Tang, 2019) (**Figs. 12, 13, 15A**). The tuffaceous turbidites were derived from volcanoes located east  
598 to northeast of the basin (Lai, L.S.-H. et al., 2018) (**Fig. 14B**), and thus are distinct and different than the  
599 magmatic events (>16–14 Ma and ~10–6 Ma) recorded in the underlying Tuluanshan Formation below the  
600 basal unconformity (**Fig. 3**). These results are consistent with the presence of north-trending volcanic arc main  
601 body identified in the offshore directly east of Taiwan based on well-defined magnetic (Shyu et al., 1996;

602 Hsieh et al., 2014) and gravity anomalies (Doo et al., 2018). We infer that the offshore volcanoes have  
603 subsequently subsided below sea level and are now being deformed in an active offshore imbricate thrust belt  
604 (Hsieh et al., 2020).

605 Based on facies interpretations above, we conclude that strata of the southern Coastal Range  
606 accumulated in a syn-orogenic, syn-collisional marine foredeep basin directly east of a steep orogenic front  
607 that formed the tectonically active western margin of the basin (**Fig. 15**). Active volcanoes east of the basin  
608 delivered distal tuffaceous turbidites during this time (~4–1 Ma), suggesting the eruptive centers shifted to the  
609 east during development of the basal unconformity and retro-foredeep system (See *Section 8.2*). The implied  
610 Plio-Pleistocene volcanoes are distinctly younger than the ~15-6 Ma volcanic arc and forearc environments  
611 recorded in the underlying Tuluanshan Formation, and may be related to a “double island arc” interpretation  
612 proposed by Yang et al. (1996).

613

#### 614 *8.2 Retro-foredeep basinal system in the Luzon forearc*

615 Results of our geologic mapping and basin reconstruction reveal that the modern topography of the  
616 Coastal Range is controlled by tightly folded and faulted rocks of a marine foredeep basin that formed on the  
617 eastern retrowedge flank of the Taiwan orogen, and later was deformed into the present configuration of  
618 regional thrust faults and related anticlinal culminations (**Figs. 2B, 16A**) (e.g., Dorsey, 1988; Lundberg and  
619 Dorsey, 1988; Chen et al., 2019). This conclusion is a departure from previous interpretations that high  
620 topographic ridges in the Coastal Range represent an inherited configuration of relatively undeformed volcanic  
621 islands and surrounding forearc, intra-arc, and backarc basins (**Figs. 2A, 16B**) (e.g., Chen, 1988a; Teng et al.,  
622 1988; Huang et al., 1995).

623 Data presented above provide evidence for east-dipping paleoslopes and olistostromal facies in the  
624 west, which pass laterally eastward into an eastward-thinning marine flysch succession that onlaps onto a  
625 gently west-dipping regional unconformity (**Figs. 12, 13**). While the observed basin geometry differs from the

626 filling style of typical forearc basins (Noda, 2016, 2018), it is similar to the architecture of the modern North  
627 Luzon Trough as seen in offshore seismic reflection studies south of Taiwan (e.g., Lundberg et al., 1997;  
628 Hirtzel et al., 2009; Chi et al., 2014). This similarity suggests that the eastward-onlapping pattern of Plio-  
629 Pleistocene orogen-derived deposits in the Coastal Range may reflect inherited, pre-collisional forearc basin  
630 bathymetry. It is also not certain that the east-dipping paleoslope at the west margin of the 4–1 Ma Coastal  
631 Range basin was controlled by east-vergent thrusts, as proposed by previous workers (e.g., Suppe and Liou,  
632 1979; Page and Suppe, 1981; Lundberg and Dorsey, 1990) and this study (**Figs. 15A, 16**), considering that the  
633 west margin of the modern North Luzon Trough does not show consistent east-vergent thrust structures (**Fig.**  
634 **1**).

635         Despite these ambiguities, several observations suggest that the modern setting is not an exact analog  
636 for the past. First, the entire Coastal Range basin subsided rapidly below sea level until ~1 Ma, as indicated by  
637 the youngest depositional age of thick marine deposits in the north-central Coastal Range (Lee, 1992; Huang  
638 et al., 2018). This requires a major tectonic reorganization that abruptly ended subsidence and initiated uplift,  
639 precluding gradual southward propagation of the collision (see also Lee et al., 2015; Hsu et al., 2016). Second,  
640 it appears the kinematic style at the east margin of the Taiwan collisional orogen may have become more  
641 transpressional in the past ca. 1 Myr during tectonic reorganization (see *section 8.4*). Third, the traditional  
642 forearc basin model cannot explain the observed sudden change in depositional age and benthic foraminiferal  
643 assemblages at the basal contact of SSS, SGS, and BBS sections (**Figs. 13, S14A-B**). In these sections the  
644 basal erosional unconformity records an age gap of ~6–4 Myr and is capped by the shallow marine Kangkou  
645 Limestone which is directly overlain by deep-water flysch (facies F1 and F2) (Huang and Yuan, 1994). These  
646 stratigraphic relations imply a dynamic history of vertical crustal motions comprising regional slow uplift and  
647 erosion of forearc volcanic basement (Tuluanshan Formation), deposition of shallow-water limestone on the  
648 eroded basement, then rapid subsidence to deep water during initiation of the collisional basin (Dorsey, 1992).  
649 The vertical crustal motions have previously been interpreted as a localized intra-arc pull-part mechanism

650 (Huang et al., 1995), but there is no field evidence for large-scale normal faults that postdate deposition of the  
651 Kangkou Limestone and predate the Paliwan Formation in the Coastal Range (Barrier and Angelier, 1986; Lin  
652 et al., 1999).

653 We therefore postulate that the asymmetric westward-deepening basin geometry represents a  
654 deflection profile produced by lithospheric flexure in response to tectonic loading in the Taiwan collisional  
655 orogen to the west (**Fig. 16A**). This is consistent with rapid sediment accumulation rates in the Coastal Range  
656 ( $\geq 1\text{-}7\text{ mm yr}^{-1}$ ) that record rapid subsidence east of the growing Taiwan collisional orogen in response to rapid  
657 thrust-loading in the orogenic thrust belt during deposition (Lundberg and Dorsey, 1988). Within this  
658 framework, the basal unconformity between the Tuluanshan Formation and overlying orogen-derived  
659 sediments is interpreted as a result of regional uplift and erosion on a broad flexural forebulge (Dorsey, 1992)  
660 (**Fig. 3**). The Kangkou Limestone and Biehchi Epiclastic Unit formed during development of the unconformity  
661 ( $\sim 6\text{-}4\text{ Ma}$ ), and they represent local thin discontinuous deposits that accumulated intermittently on the flexural  
662 forebulge. These relationships suggest rapid subsidence in response to an eastward migrating wave of flexural  
663 depression that is a common aspect of foreland basin evolution (DeCelles and Giles, 1996; DeCelles, 2012).

664 This hypothesis is consistent with the observed eastward progradation of coarse-sediment facies  
665 including mass-wasting deposits (X1 and X3) and channelized gravelly sediment gravity-flow deposits (F3  
666 and F4), which are best explained as the result of basinward migration of the depocenter in response to an  
667 eastward advancing submarine slope at the retrowedge orogenic front, likely caused by a series of east-vergent  
668 thrusts (**Figs. 15A, 16A**). This pattern represents a marine analog to migrating coarse-sediment facies that are  
669 commonly interpreted as a response to a migrating flexural wave in terrestrial foreland basins (Heller et al.,  
670 1988; Sinclair, 2012; Dubille and Lavé, 2015).

671 Lithofacies of the Tuluanshan Formation beneath the basal unconformity (**Fig. 3**) make up a sequence  
672 of volcanic and volcanoclastic rocks that record underwater to subaerial eruptions within and on the flanks of  
673 late Miocene ( $\sim 15\text{-}6\text{ Ma}$ ) subduction-related arc volcanoes (Chen, 1997a; Song and Lo, 2002; Lai and Song,

674 2013). This suggests that the Plio-Pleistocene retro-foredeep basin of the Coastal Range formed on top of older,  
675 deeply subsided crust of an inactive Luzon Arc, similar to the modern retro-foredeep in the North Luzon  
676 Trough offshore of southeastern Taiwan (**Fig. 1A**). In the modern southeast offshore region, a unique  
677 collisional foredeep basin is forming where the forearc is closing due to the transition from intra-oceanic  
678 subduction to a mature arc-continent collision (e.g., Lundberg et al., 1997; Hirtzel et al., 2009).

679

### 680 *8.3 Genesis and distribution of the Lichi Mélange*

681 All published studies agree that the modern expression and distribution of the Lichi Mélange are  
682 influenced by tectonic shearing related to faults in the western Coastal Range that have been active in the past  
683 ca. 1 Myr (e.g., Page and Suppe, 1981; Chang et al., 2000). However, there is a considerable debate over the  
684 question of whether sedimentary processes (e.g., sliding and slumping) were involved in formation of this  
685 mélange (Teng, 1981; Chen, 1997b; Huang et al., 2018). This study confirms the ubiquitous presence of  
686 depositional contacts and interbedding between Lichi Mélange and Plio-Pleistocene orogen-derived flysch  
687 facies of the Fanshuliao and Paliwan formations (**Figs. 8, 10**). Young (~4–1 Ma) microfossils coexist among  
688 these sedimentary units in the southern Coastal Range (**Fig. 11**), providing an important new constraint on this  
689 question. Our data show that the Lichi Mélange was generated by olistostromal and mass-wasting processes  
690 (**Fig. 15**). We also observe evidence of overprinting tectonic shear fabrics and fault-zone breccias produced by  
691 post-depositional, cross-cutting, west-vergent thrust faults including the Tuluanshan fault (**Figs. 4, 8**). This  
692 late-stage structural disturbance is currently active along the strands of the active Longitudinal Valley fault  
693 (Angelier et al., 2000; Lee et al., 2006). The structural fabrics related to young deformation are mainly  
694 restricted to brittle damage zones within and adjacent to the faults, and they are volumetrically minor compared  
695 to widespread sedimentary features and depositional contacts that are commonly observed in the Lichi  
696 Mélange (Page and Suppe, 1981; Barrier and Muller, 1984).

697 Based on evidence presented above, we propose a polygenetic model for evolution of the Lichi  
698 Mélange in eastern Taiwan (**Fig. 16A**). During the growth of orogenic topography between  $\sim 6$  and 1 Ma,  
699 eastward propagating thrust faults drove basinward migration of a steep submarine slope at the advancing  
700 retrowedge front of the collisional orogen (e.g., Malavieille et al., 2021) (**Fig. 16A-1, A-2**). Thrust-controlled  
701 slope oversteepening resulted in slope failures, slides, and slumps that produced olistostrome deposits at the  
702 western margin of a syn-orogenic marine foredeep basin formed on older inactive arc and forearc crust (**Fig.**  
703 **15A**). During the advance of the orogenic thrust front, older olistostromes and associated sediments may be  
704 reworked into the frontal slope to produce new olistostromes, thus forming an “olistostromal carpet” (see Festa  
705 et al., 2010 and references therein). Later, the olistostrome deposits were overprinted by post-depositional  
706 tectonic fault zones associated with the Tuluanshan and Longitudinal Valley faults (**Fig. 16A-3**). The young,  
707 post-1 Ma stage of active deformation and rapid uplift inverted the foredeep basin along west-vergent thrusts  
708 in the Coastal Range (Lundberg and Dorsey, 1990), rapidly constructed steep rugged topography of the modern  
709 Coastal Range, and overprinted the Lichi Mélange to form a polygenetic mélange.

710 Our interpretation for the Lichi Mélange contrasts with a popular model proposed in prior studies, in  
711 which the Lichi Mélange solely formed by tectonic shearing of older sedimentary rocks in an east-vergent then  
712 west-vergent mega-thrust zone as a result of large-scale tectonic shortening in the forearc region (e.g., Chen,  
713 1997b; Chang et al., 2001; Huang et al., 2018) (**Fig. 16B**). New constraints on the age, contacts, map relations,  
714 interbedding, and sedimentary facies associations (this study) contradict the “tectonic-only” mélange model,  
715 and clearly require emplacement by submarine mass wasting. Some workers suggest that preservation of the  
716 Lichi Mélange in the western belt of the southern Coastal Range indicates that it formed as a tectonic mélange  
717 produced entirely by fault zone deformation (Teng, 1981; Chen, 1991; Huang et al., 2018). However, the  
718 affinity of mélange to fault zones only suggests the likelihood of structural overprints, and does not provide  
719 evidence for its origin (Festa et al., 2019; Raymond, 2019; Wakabayashi, 2019). In fact, abundant olistostromal  
720 facies such as slump beds (X2), pebbly mudstone (X1), and olistoliths (X4) are also reported close to mapped

721 patches of Lichi Mélange in the northern Coastal Range (e.g., Dorsey and Lundberg, 1988; Song et al., 1994;  
722 Teng et al., 2002), suggesting that deposits associated with the sedimentary mélange are common in the  
723 northern Coastal Range as well.

724 The extent to which tectonic deformation has been absorbed in the present form of the Lichi Mélange  
725 remains unclear. It is plausible that post-depositional structures (both pre-1 Ma east-vergent thrusts and post-  
726 1 Ma west-vergent thrusts) influenced some of the shear surfaces formed by preceding olistostromal processes  
727 (**Fig. 16A-2, A-3**). Further meso-scale and microscopic studies of shear fabrics in the mélange matrix are  
728 needed to address this question.

729

#### 730 *8.4 Crustal shortening and tectonic recycling at the suture of an arc-continent collision*

731 Because the Lichi Mélange formed primarily by sedimentary mass-wasting processes, the belt of rocks  
732 mapped as this mélange should not be considered as a “mega-thrust” zone that absorbs most of the crustal  
733 shortening associated with accretion of the Luzon Arc (e.g., Teng, 1987; Chen, 1997b; Chang et al., 2001;  
734 Huang et al., 2008). Tectonic horizontal shortening within the Coastal Range is primarily taken up by structures  
735 of the west-vergent fold-and-thrust belt that initiated ca. 1 Ma and post-date deposition in the Coastal Range  
736 foredeep basin (Chi et al., 1981; Dorsey, 1992). In addition, convergence on the oblique west-vergent  
737 Longitudinal Valley fault, and east-vergent thrust belt offshore of eastern Taiwan (e.g., Huang et al., 2010;  
738 Hsieh et al., 2020), suggests that the Coastal Range is an active doubly-vergent transpressional wedge within  
739 the active collisional suture between the Eurasian and Philippine Sea plates (e.g., Malavieille et al., 2016;  
740 Thomas et al., 2014) (**Figs. 16A**). Similar doubly-vergent wedge structures have been reported in the northern  
741 Coastal Range (e.g., Yen et al., 2018), directly offshore to the east (Hsieh et al., 2020), and the Huatung Ridge  
742 in southern offshore (e.g., Huang et al., 2000; Hirtzel et al., 2009; Chi et al., 2014) (**Figs. 1A**).

743 Our data confirm that exotic blocks in olistostromes of the Lichi Mélange, and variably rounded clasts  
744 of associated debris flow deposits, contain a diverse set of lithologies including arc-related andesite, andesitic

745 volcaniclastic sandstone, limestone, ophiolitic rocks (gabbro, serpentinite, granodiorite), low-grade  
746 metasediments, slate fragments, and Miocene quartz-rich sandstones that represent fragments of the Eurasian  
747 and Philippine Sea plates. This observation, combined with widespread evidence for east- and southeast-  
748 dipping paleoslopes, indicates that all of these rock types were exposed and deformed in thrust sheets in the  
749 eastern retro-wedge of the Taiwan collisional orogen (**Fig. 16A**). We propose that many of these rock  
750 lithologies represent shallow-crustal equivalents of high-P greenschist to blueschist grade metamorphic rocks  
751 in the Yuli Belt, which occupies the easternmost belt of the metamorphic Central Range belt directly west of  
752 the Coastal Range (**Figs. 1, 16A**). The Yuli Belt was recently recognized as a metamorphosed late-Miocene (~  
753 6–9 Ma) mélangé (Chen, W.-S. et al., 2017; Mesalles et al., 2020) that contains Miocene mafic and ultramafic  
754 fragments of the South China Sea as well as arc-affinity metavolcanic rocks (e.g., Jahn and Liou, 1977; Sun et  
755 al., 1998). Unmetamorphosed equivalents of similar aged low-grade meta-sediments (i.e., Eastern Slates)  
756 adjacent to the Yuli Belt (**Fig. 1A**), interpreted as a former forearc basin sequence (e.g., Stanley et al., 1981;  
757 Mesalles, 2014), represent the likely source of exotic Miocene sedimentary blocks in the Lichi Mélangé (Chi  
758 et al., 1981). This idea is supported by the distinctive quartz-rich petrography of exotic sandstone blocks, which  
759 closely resembles that of sedimentary rocks now exposed at the south end of the Eastern Slate belt on the  
760 Hengchun peninsula (Sung, 1991).

761         These results suggest that volcanic arc and forearc crustal fragments of the oceanic Philippine Sea plate  
762 were tectonically recycled into the eastern retrowedge of the collisional orogen, likely by accretion and/or  
763 underplating within a subduction zone or subduction channel complex. This took place during deposition of  
764 the Lichi Mélangé, prior to final closure of the retro-foredeep basin (Suppe and Liou, 1979; Page and Suppe,  
765 1981; Malavieille et al., 2016). A modern analog may be seen in the Timor arc-continent collision system,  
766 where a retro-foredeep basin is currently active in the Banda forearc region and fragments of the Banda Arc  
767 crust have already been emplaced in the Bobonaro Mélangé in the retrowedge sector of the active Timor  
768 collisional orogen (e.g., Harris et al., 1998; Tate et al., 2015). Another comparable example of tectonically



769 reworked olistostromes that formed in the retrowedge of a collisional orogen is well-documented in the late  
770 Cretaceous – Eocene northern Apennine belt in Italy (e.g., Malavieille et al., 2016; Barbero et al., 2020).

771 During the past ca. 1 Myr, the Lichi Mélange and retro-foredeep strata of the Coastal Range have been  
772 rapidly uplifted, imbricated, and incorporated along with underlying volcanic arc crust into the leading edge  
773 of the modern collisional orogen (**Fig. 16A**). These rocks are now part of a new, rapidly uplifting emergent  
774 mountain range that represents a potential source for a new generation of mélangé formation (either tectonic  
775 or sedimentary). This large-scale mechanism of arc crustal shortening and tectonic recycling at the ocean-  
776 continent interface of a doubly-vergent collisional orogen may be a general process in the formation of  
777 polygenetic mélangé in arc-continent collision systems, which play a critical role in the growth of continental  
778 lithosphere through time (Clift et al., 2008; Draut and Clift, 2012).

779

## 780 **9. Conclusions**

781 Our multidisciplinary study confirms a sedimentary origin for the ca. 4–1 Ma Lichi Mélange in the  
782 southern Coastal Range of eastern Taiwan. This unit formed by submarine slope failures, slides, slumps, and  
783 debris flows that interfinger laterally with a coeval thick (ca. 4–7 km) succession of turbidite-dominated flysch  
784 deposits that filled a syn-orogenic marine retro-foredeep basin. The entire syn-collisional succession overlies  
785 and onlaps eastward onto a regional unconformity that formed by erosion of older, late Miocene volcanic-arc  
786 and forearc-basin deposits. Major arc volcanism recorded in the Miocene Tuluanshan Formation ceased prior  
787 to the onset of eastward migrating subsidence, which we infer took place in front of the east-vergent retrowedge  
788 of the collisional orogen. Minor tuffaceous turbidites in the post-Miocene flysch sequence record input from a  
789 different, younger volcanic source that was located offshore to the east during Plio-Pleistocene basin  
790 development. Diverse rock types in Lichi Mélange blocks and clasts of associated debris flow deposits indicate  
791 that arc and forearc crustal fragments of the oceanic Philippine Sea plate were tectonically recycled into the

792 eastern retrowedge belt of the collisional orogen during the 4–1 Ma formation of the Lichi Mélange and  
793 associated flysch deposits near the tectonically controlled western margin of the basin.

794         During the past ca. 1 Myr, the Lichi Mélange and retro-foredeep strata of the Coastal Range have been  
795 rapidly uplifted, deformed, and incorporated into the ocean-facing margin of the modern collisional orogen  
796 along with underlying Miocene volcanic arc crust. The present-day expression of the Lichi Mélange is  
797 modified by structural overprints and fault-zone fabrics, but the mélange itself did not form solely by fault-  
798 zone processes. It is a complex association of olistostromes emplaced by large submarine slides and slumps  
799 derived from the eastern retrowedge of the Taiwan collisional orogen. These results reveal a dynamic and  
800 complicated history of mélange-forming processes in respond to frequent rock mixing and reworking at the  
801 oceanic interface of an active arc-continent collision. Similarity between our findings in eastern Taiwan and  
802 other polygenetic mélanges associated with retrowedge basins suggests that long-term tectonic recycling  
803 associated with crustal shortening may be a common process in retrowedge foredeep basins of active  
804 collisional orogens, particularly in (but not limited to) arc-continent collision systems.

805

## 806 **Acknowledgements**

807         We appreciate valuable reviews by Andrea Festa and an anonymous reviewer, and an informal review  
808 by John Suppe, which greatly improved this manuscript. We thank Chien-Hao Wang, Kuan-Yu Wang, Ping-  
809 Chuan Chen, and Charlie Ogle for field assistance, and Kuo-Hang Chen, Chun-Hung Lin for collecting and  
810 processing samples for paleomagnetism and nannofossil analyses. This research was funded by the Geological  
811 Society of America (2018 Graduate Student Research Grant) and the Ministry of Science and Technology of  
812 Taiwan (MOST 107-2811-M-259-002).

813

## 814 **References**

815 Abbate, E., Bortolotti, V., Passerini, P., 1970. Olistostromes and olistoliths. *Sedimentary Geology* 4, 521-557.



- 816 Angelier, J., Chu, H.-T., Lee, J.-C., Hu, J.-C., 2000. Active faulting and earthquake risk: the Chihshang Fault case,  
817 Taiwan. *Journal of Geodynamics* 29, 151-185.
- 818 Anthonissen, D.E., Ogg, J.G., 2012. Appendix 3 - Cenozoic and Cretaceous biochronology of planktonic  
819 foraminifera and calcareous nannofossils. In: Gradstein, F.M., Ogg, J.G., Schmitz, M.D., Ogg, G.M. (Eds.),  
820 *The Geologic Time Scale 2012*. Elsevier, Boston, USA, pp. 1083-1127.
- 821 Backman, J., Raffi, I., Rio, D., Fornaciari, E., Pälke, H., 2012. Biozonation and biochronology of Miocene through  
822 Pleistocene calcareous nannofossils from low and middle latitudes. *Newsletters on Stratigraphy* 45, 221-244.
- 823 Barbero, E., Festa, A., Saccani, E., Catanzariti, R., D'Onofrio, R., 2020. Redefinition of the Ligurian Units at the  
824 Alps–Apennines junction (NW Italy) and their role in the evolution of the Ligurian accretionary wedge:  
825 constraints from mélanges and broken formations. *Journal of the Geological Society* 177, 562-574.
- 826 Barrier, E., Muller, C., 1984. New observations and discussion on the origin and age of the Lichi Mélange. *Memoir*  
827 *of the Geological Society of China* 6, 303-325.
- 828 Barrier, E., Angelier, J., 1986. Active collision in eastern Taiwan: the Coastal Range. *Tectonophysics* 125, 39-72.
- 829 Beyssac, O., Negro, F., Simoes, M., Chan, Y.C., Chen, Y.G., 2008. High-pressure metamorphism in Taiwan: from  
830 oceanic subduction to arc-continent collision? *Terra Nova* 20, 118-125.
- 831 Biq, C.C., 1977. The Kenting Mélange and the Manila Trench. *Proceedings of the Geological Society of China* 20,  
832 119-122.
- 833 Buchovecky, E.J., Lundberg, N., 1988. Clay mineralogy of mudstones from the southern Coastal Range, eastern  
834 Taiwan: Unroofing of the orogen versus in-situ diagenesis. *Acta Geologica Taiwanica: Science Reports of the*  
835 *National Taiwan University* 26, 247-261.
- 836 Chang, C.-P., Angelier, J., Huang, C.-Y., 2000. Origin and evolution of a melange: the active plate boundary and  
837 suture zone of the Longitudinal Valley, Taiwan. *Tectonophysics* 325, 43-62.
- 838 Chang, C.-P., Angelier, J., Huang, C.-Y., Liu, C.-S., 2001. Structural evolution and significance of a melange in a  
839 collision belt: the Lichi Melange and the Taiwan arc-continent collision. *Geological Magazine* 138, 633-651.
- 840 Chang, L.S., 1967. A biostratigraphic study of the Tertiary in the Coastal Range, eastern Taiwan, based on smaller  
841 foraminifera (I: southern part). *Proceedings of the Geological Society of China* 10, 64-76.

- 842 Chang, L.S., 1969. A biostratigraphic study of the Tertiary in the Coastal Range, eastern Taiwan, based on smaller  
843 foraminifera (III: middle part). *Proceedings of the Geological Society of China* 12, 89-101.
- 844 Chen, T.-W., Chung, S.-L., Chen, W.-S., 2015. Zircon U-Pb geochronology of the Plio-Pleistocene volcanogenic  
845 and orogenic sedimentary rocks from the Coastal Range, eastern Taiwan. EGU General Assembly, 12-17 April,  
846 2015, Vienna, Austria. Abstract #EGU2015-7818-1.
- 847 Chen, W.-H., Huang, C.-Y., Lin, Y.-J., Zhao, Q., Yan, Y., Chen, D., Zhang, X., Lan, Q., Yu, M., 2015. Depleted  
848 deep South China Sea  $\delta^{13}\text{C}$  paleoceanographic events in response to tectonic evolution in Taiwan–Luzon Strait  
849 since Middle Miocene. *Deep Sea Research Part II: Topical Studies in Oceanography* 122, 195-225.
- 850 Chen, W.-H., Huang, C.-Y., Yan, Y., Dilek, Y., Chen, D., Wang, M.-H., Zhang, X., Lan, Q., Yu, M., 2017.  
851 Stratigraphy and provenance of forearc sequences in the Lichi Mélange, Coastal Range: Geological records of  
852 the active Taiwan arc-continent collision. *Journal of Geophysical Research: Solid Earth* 122, 7408-7436.
- 853 Chen, W.-S., 1988a. Development of deep-sea fan systems in Coastal Range basin, eastern Taiwan. *Acta Geologica*  
854 *Taiwanica: Science Reports of the National Taiwan University* 26, 37-56.
- 855 Chen, W.-S., 1988b. Tectonic Evolution of Sedimentary Basins in Coastal Range, Taiwan (Ph.D. thesis). National  
856 Taiwan University, Taipei, Taiwan, 344 pp. (in Chinese).
- 857 Chen, W.-S., 1991. Origin of the Lichi Melange in the Coastal Range, eastern Taiwan. Special Publication of the  
858 Central Geological Survey, MOEA 5, 257-266. (in Chinese with English abstract).
- 859 Chen, W.-S., 1997a. Lithofacies analyses of the arc-related sequence in the Coastal Range, eastern Taiwan. *Journal*  
860 *of the Geological Society of China* 40, 313-338.
- 861 Chen, W.-S., 1997b. Mesoscopic structures developed in the Lichi melange during arc-continent collision in Taiwan  
862 region. *Journal of the Geological Society of China* 40, 415-434.
- 863 Chen, W.-S., 2009. Tectonostratigraphic framework and age of the volcanic-arc and collision basins in the Coastal  
864 Range, eastern Taiwan. *Western Pacific Earth Sciences* 9, 67-98 (in Chinese with English abstract).
- 865 Chen, W.-S., Lin, I.-C., Yen, Y.-C., Yang, C.-C., Chi, C.-Y., Huang, N.-W., Lin, C.-W., Lin, W.-S., Hou, C.-S.,  
866 Liu, Y.-C., Lin, Y.-H., Shih, T.-S., Lu, S.-T., 2008. Fault segmentation of the Longitudinal Valley Fault in

- 867 eastern Taiwan: Evidence from paleoseismic investigations and GPS observations. Special Publication of the  
868 Central Geological Survey, MOEA 20, 165-191. (in Chinese with English abstract).
- 869 Chen, W.-S., Chung, S.-L., Chou, H.-Y., Zugeerbai, Z., Shao, W.-Y., Lee, Y.-H., 2017. A reinterpretation of the  
870 metamorphic Yuli belt: Evidence for a middle-late Miocene accretionary prism in eastern Taiwan. *Tectonics*  
871 36, 188-206. <https://doi.org/10.1002/2016TC004383>.
- 872 Chen, W.-S., Yeh, J.-J., Syu, S.-J., 2019. Late Cenozoic exhumation and erosion of the Taiwan orogenic belt: New  
873 insights from petrographic analysis of foreland basin sediments and thermochronological dating on the  
874 metamorphic orogenic wedge. *Tectonophysics* 750, 56-69.
- 875 Chen, W.-S., Yang, C.-Y., Chen, S.-T., Huang, Y.-C., 2020. New insights into Holocene marine terrace  
876 development caused by seismic and aseismic faulting in the Coastal Range, eastern Taiwan. *Quaternary Science*  
877 *Reviews* 240, 106369. <https://doi.org/10.1016/j.quascirev.2020.106369>.
- 878 Chi, W.-C., Chen, L., Liu, C.-S., Brookfield, M., 2014. Development of arc–continent collision mélanges: Linking  
879 onshore geological and offshore geophysical observations of the Pliocene Lichi Mélange, southern Taiwan and  
880 northern Luzon arc, western Pacific. *Tectonophysics* 636, 70-82.
- 881 Chi, W.-R., Namson, J., Suppe, J., 1981. Stratigraphic record of plate interactions in the Coastal Range of eastern  
882 Taiwan. *Memoir of the Geological Society of China* 4, 155-194.
- 883 Chuang, C.-K., Lo, L., Zeeden, C., Chou, Y.-M., Wei, K.-Y., Shen, C.-C., Mii, H.-S., Chang, Y.-P., Tung, Y.-H.,  
884 2018. Integrated stratigraphy of ODP Site 1115 (Solomon Sea, southwestern equatorial Pacific) over the past  
885 3.2 Ma. *Marine Micropaleontology* 144, 25-37.
- 886 Clift, P.D., Vannucchi, P., 2004. Controls on tectonic accretion versus erosion in subduction zones: Implications  
887 for the origin and recycling of the continental crust. *Reviews of Geophysics* 42, RG2001.  
888 <https://doi.org/10.1029/2003RG000127>.
- 889 Clift, P.D., Lin, A.T.S., Carter, A., Wu, F., Draut, A.E., Lai, T.H., Fei, L.Y., Schouten, H., Teng, L., 2008. Post-  
890 collisional collapse in the wake of migrating arc-continent collision in the Ilan Basin, Taiwan. In: Draut, A.E.,

- 891 Clift, P.D., Scholl, D.W. (Eds.), Formation and Applications of the Sedimentary Record in Arc Collision Zones.  
892 The Geological Society of America Special Papers 436, pp. 257-278.
- 893 Codegone, G., Festa, A., Dilek, Y., Pini, G.A., 2012. Small-scale polygenetic mélanges in the Ligurian accretionary  
894 complex, Northern Apennines, Italy, and the role of shale diapirism in superposed mélange evolution in  
895 orogenic belts. *Tectonophysics* 568-569, 170-184.
- 896 Conand, C., Mouthereau, F., Ganne, J., Lin, A.T.-S., Lahfid, A., Daudet, M., Mesalles, L., Giletycz, S., Bonzani,  
897 M., 2020. Strain partitioning and exhumation in oblique Taiwan collision: Role of rift architecture and plate  
898 kinematics. *Tectonics* 39, e2019TC005798. <https://doi.org/10.1029/2019tc005798>.
- 899 Cowan, D.S., 1985. Structural styles in Mesozoic and Cenozoic mélanges in the western Cordillera of North  
900 America. *Geological Society of America Bulletin* 96, 451-462.
- 901 DeCelles, P.G., 2012. Foreland basin systems revisited: Variations in response to tectonic settings. In: Busby, C.,  
902 Azor, A. (Eds.), *Tectonics of Sedimentary Basins: Recent Advances*. Blackwell Publishing Ltd., Oxford, UK,  
903 pp. 405-426.
- 904 DeCelles, P.G., Giles, K.A., 1996. Foreland basin systems. *Basin Research* 8, 105-123.
- 905 Dilek, Y., Festa, A., Ogawa, Y., Pini, G.A., 2012. Chaos and geodynamics: Mélanges, mélange-forming processes  
906 and their significance in the geological record. *Tectonophysics* 568-569, 1-6.
- 907 Doo, W.-B., Lo, C.-L., Hsu, S.-K., Tsai, C.-H., Huang, Y.-S., Wang, H.-F., Chiu, S.-D., Ma, Y.-F., Liang, C.-W.,  
908 2018. New gravity anomaly map of Taiwan and its surrounding regions with some tectonic interpretations.  
909 *Journal of Asian Earth Sciences* 154, 93-100.
- 910 Dorsey, R.J., 1985. Petrography of Neogene sandstones from the Coastal Range of eastern Taiwan: response to arc-  
911 continent collision. *Petroleum Geology of Taiwan* 21, 187-215.
- 912 Dorsey, R.J., 1988. Provenance evolution and unroofing history of a modern arc-continent collision: Evidence from  
913 petrography of Plio-Pleistocene sandstones, eastern Taiwan. *Journal of Sedimentary Research* 58, 208-218.
- 914 Dorsey, R.J., 1992. Collapse of the Luzon volcanic arc during onset of arc-continent collision: Evidence from a  
915 Miocene-Pliocene unconformity, eastern Taiwan. *Tectonics* 11, 177-191.

- 916 Dorsey, R.J., Lundberg, N., 1988. Lithofacies analysis and basin reconstruction of the Plio-Pleistocene collisional  
917 basin, Coastal Range of eastern Taiwan. *Acta Geologica Taiwanica Science Reports of the National Taiwan*  
918 *University* 26, 57-132.
- 919 Dorsey, R.J., Buchovecky, E.J., Lundberg, N., 1988. Clay mineralogy of Pliocene-Pleistocene mudstones, eastern  
920 Taiwan: Combined effects of burial diagenesis and provenance unroofing. *Geology* 16, 944-947.
- 921 Draut, A.E., Clift, P.D., 2012. Basins in arc-continental collisions. In: Cathy, B., Antonio, A. (Eds.), *Tectonics of*  
922 *Sedimentary Basins: Recent Advances*. Blackwell Publishing Ltd., Oxford, UK, pp. 347-368.
- 923 Draut, A.E., Clift, P.D., 2013. Differential preservation in the geologic record of intraoceanic arc sedimentary and  
924 tectonic processes. *Earth-Science Reviews* 116, 57-84.
- 925 Dubille, M., Lavé, J., 2015. Rapid grain size coarsening at sandstone/conglomerate transition: similar expression in  
926 Himalayan modern rivers and Pliocene molasse deposits. *Basin Research* 27, 26-42.
- 927 Ernst, W.G., 1977. Olistostromes and included ophiolitic debris from the Coastal Range of eastern Taiwan. *Memoir*  
928 *of the Geological Society of China* 2, 97-114.
- 929 Festa, A., Pini, G.A., Dilek, Y., Codegone, G., 2010. Mélanges and mélange-forming processes: a historical  
930 overview and new concepts. *International Geology Review* 52, 1040-1105.
- 931 Festa, A., Dilek, Y., Pini, G.A., Codegone, G., Ogata, K., 2012. Mechanisms and processes of stratal disruption and  
932 mixing in the development of mélanges and broken formations: Redefining and classifying mélanges.  
933 *Tectonophysics* 568-569, 7-24.
- 934 Festa, A., Ogata, K., Pini, G.A., Dilek, Y., Alonso, J.L., 2016. Origin and significance of olistostromes in the  
935 evolution of orogenic belts: A global synthesis. *Gondwana Research* 39, 180-203.
- 936 Festa, A., Pini, G.A., Ogata, K., Dilek, Y., 2019. Diagnostic features and field-criteria in recognition of tectonic,  
937 sedimentary and diapiric mélanges in orogenic belts and exhumed subduction-accretion complexes. *Gondwana*  
938 *Research* 74, 7-30.
- 939 Festa, A., Ogata, K., Pini, G.A., 2020. Polygenetic mélanges: a glimpse on tectonic, sedimentary and diapiric  
940 recycling in convergent margins. *Journal of the Geological Society* 177, 551-561.

- 941 Fisher, D.M., Willett, S., Yeh, E.-C., Clark, M.B., 2007. Cleavage fronts and fans as reflections of orogen stress  
942 and kinematics in Taiwan. *Geology* 35, 65-68. <https://doi.org/10.1130/g22850a.1>.
- 943 Fisher, R.A., 1953. Dispersion on a sphere. *Proceedings of the Royal Society of London. Series A. Mathematical*  
944 *and Physical Sciences* 217, 295-305.
- 945 Greenly, E., 1919. *The Geology of Anglesey*: London. Geological Survey of Great Britain. Her Majesty's Stationery  
946 Office, Richmond, UK, 980 pp.
- 947 Harris, R.A., Audley-Charles, M.G., 1987. Taiwan and Timor neotectonics: A comparative review. *Memoir of the*  
948 *Geological Society of China* 9, 45-61.
- 949 Harris, R.A., Sawyer, R.K., Audley-Charles, M.G., 1998. Collisional melange development: Geologic associations  
950 of active melange-forming processes with exhumed melange facies in the western Banda orogen, Indonesia.  
951 *Tectonics* 17, 458-479.
- 952 Heller, P.L., Angevine, C.L., Winslow, N.S., Paola, C., 1988. Two-phase stratigraphic model of foreland-basin  
953 sequences. *Geology* 16, 501-504.
- 954 Hirtzel, J., Chi, W.C., Reed, D., Chen, L., Liu, C.S., Lundberg, N., 2009. Destruction of Luzon forearc basin from  
955 subduction to Taiwan arc–continent collision. *Tectonophysics* 479, 43-51.
- 956 Ho, C.S., 1977. Mélanges in the Neogene sequence of Taiwan. *Memoir of the Geological Society of China* 2, 85-  
957 96.
- 958 Horng, C.S., Shea, K.S., 1996. Dating of the Plio-Pleistocene rapidly deposited sequence based on integrated  
959 magneto-biostratigraphy: a case study of the madagida-chi section, coastal range, eastern Taiwan. *Journal of*  
960 *the Geological Society of China* 39, 31-58.
- 961 Hsieh, H.-H., Chen, C.-H., Lin, P.-Y., Yen, H.-Y., 2014. Curie point depth from spectral analysis of magnetic data  
962 in Taiwan. *Journal of Asian Earth Sciences* 90, 26-33.
- 963 Hsieh, M.-L., Rau, R.-J., 2009. Late Holocene coseismic uplift on the Hua-tung coast, eastern Taiwan: Evidence  
964 from mass mortality of intertidal organisms. *Tectonophysics* 474, 595-609.



- 965 Hsieh, Y.-H., Liu, C.-S., Suppe, J., Byrne, T.B., Lallemand, S., 2020. The Chimei submarine canyon and fan: A  
966 record of Taiwan arc-continent collision on the rapidly deforming over-riding plate. *Tectonics* 39,  
967 e2020TC006148. <https://doi.org/10.1029/2020TC006148>.
- 968 Hsü, K.J., 1968. Principles of mélanges and their bearing on the Franciscan-Knoxville paradox. *Geological Society*  
969 *of America Bulletin* 79, 1063-1074.
- 970 Hsü, K.J., 1988. Mélange and the mélange tectonics of Taiwan. *Proceedings of the Geological Society of China* 31,  
971 87-92.
- 972 Hsu, T.L., 1956. Geology of the Coastal Range, eastern Taiwan. *Bulletin of the Central Geological Survey of*  
973 *Taiwan* 8, 39-63.
- 974 Hsu, W.-H., Byrne, T.B., Ouimet, W., Lee, Y.-H., Chen, Y.-G., van Soest, M., Hodges, K., 2016. Pleistocene onset  
975 of rapid, punctuated exhumation in the eastern Central Range of the Taiwan orogenic belt. *Geology* 44, 719-  
976 722.
- 977 Huang, C.-Y., Yuan, P.B., 1994. Stratigraphy of the Kangkou Limestone in the Coastal Range, eastern Taiwan.  
978 *Journal of Geological Society of China* 37, 585-605.
- 979 Huang, C.-Y., Yuan, P.B., Song, S.-R., Lin, C.W., Wang, C.S., Chen, M.T., Shyu, C.T., Karp, B., 1995. Tectonics  
980 of short-lived intra-arc basins in the arc-continent collision terrane of the Coastal Range, eastern Taiwan.  
981 *Tectonics* 14, 19-38.
- 982 Huang, C.-Y., Wu, W.Y., Chang, C.-P., Tsao, S., Yuan, P.B., Lin, C.W., Xia, K.Y., 1997. Tectonic evolution of  
983 accretionary prism in the arc-continent collision terrane of Taiwan. *Tectonophysics* 281, 31-51.
- 984 Huang, C.-Y., Yuan, P.B., Lin, C.-W., Wang, T.K., Chang, C.-P., 2000. Geodynamic processes of Taiwan arc-  
985 continent collision and comparison with analogs in Timor, Papua New Guinea, Urals and Corsica.  
986 *Tectonophysics* 325, 1-21.
- 987 Huang, C.-Y., Yuan, P.B., Tsao, S.-J., 2006. Temporal and spatial records of active arc-continent collision in  
988 Taiwan: A synthesis. *Geological Society of America Bulletin* 118, 274-288.
- 989 Huang, C.-Y., Chien, C.-W., Yao, B., Chang, C.-P., 2008. The Lichi Mélange: A collision mélange formation along  
990 early arcward backthrusts during forearc basin closure, Taiwan arc-continent collision. In: Draut, A.E., Clift,

- 991 P.D., Scholl, D.W. (Eds.), Formation and Applications of the Sedimentary Record in Arc Collision Zones.  
992 Geological Society of America Special Paper 436, pp. 127-154.
- 993 Huang, C.-Y., Chen, W.-H., Wang, M.-H., Lin, C.-T., Yang, S., Li, X., Yu, M., Zhao, X., Yang, K.-M., Liu, C.-S.,  
994 Hsieh, Y.-H., Harris, R., 2018. Juxtaposed sequence stratigraphy, temporal-spatial variations of sedimentation  
995 and development of modern-forming forearc Lichi Mélange in North Luzon Trough forearc basin onshore and  
996 offshore eastern Taiwan: An overview. *Earth-Science Reviews* 182, 102-140.
- 997 Huang, W.-J., Johnson, K.M., Fukuda, J.i., Yu, S.-B., 2010. Insights into active tectonics of eastern Taiwan from  
998 analyses of geodetic and geologic data. *Journal of Geophysical Research: Solid Earth* 115, B03413.  
999 <https://doi.org/10.1029/2008JB006208>.
- 1000 Jahn, B.M., Liou, J.G., 1977. Age and geochemical constraints of glaucophane schists of taiwan. *Memoir of the*  
1001 *Geological Society of China* 2, 129-140.
- 1002 Keyser, W., Tsai, C.-H., Iizuka, Y., Oberhänsli, R., Ernst, W.G., 2016. High-pressure metamorphism in the  
1003 Chinshuichi area, Yuli belt, eastern Taiwan. *Tectonophysics* 692, Part B, 191-202.
- 1004 Kirstein, L.A., Fellin, M.G., Willett, S.D., Carter, A., Chen, Y.-G., Graver, J.I., Lee, D.C., 2009. Pliocene onset of  
1005 rapid exhumation in Taiwan during arc-continent collision: new insights from detrital thermochronometry.  
1006 *Basin Research* 22, 270-285.
- 1007 Kirstein, L.A., Carter, A., Chen, Y.-G., 2014. Impacts of arc collision on small orogens: new insights from the  
1008 Coastal Range detrital record, Taiwan. *Journal of the Geological Society, London* 171, 5-8.
- 1009 Kusky, T., Wang, J., Wang, L., Huang, B., Ning, W., Fu, D., Peng, H., Deng, H., Polat, A., Zhong, Y., Shi, G.,  
1010 2020. Mélanges through time: Life cycle of the world's largest Archean mélange compared with Mesozoic and  
1011 Paleozoic subduction-accretion-collision mélanges. *Earth-Science Reviews* 209, 103303.  
1012 <https://doi.org/10.1016/j.earscirev.2020.103303>.
- 1013 Lai, L.S.-H., Teng, L.S.-Y., 2016. Stratigraphy and structure of the Tai-Yuan basin, southern Coastal Range, eastern  
1014 Taiwan. *Bulletin of the Central Geological Survey, MOEA* 29, 45-76. (in Chinese with English abstract).

- 1015 Lai, L.S.-H., Ng, T.-W., Teng, L.S.-Y., 2018. Stratigraphic correlation of tuffaceous and psephitic strata in the  
1016 Paliwan formation, southern Coastal Range of eastern Taiwan. Bulletin of the Central Geological Survey,  
1017 MOEA 31, 1-32. (in Chinese with English abstract).
- 1018 Lai, Y.-M., Song, S.-R., 2013. The volcanoes of an oceanic arc from origin to destruction: A case from the northern  
1019 Luzon Arc. *Journal of Asian Earth Sciences* 74, 97-112.
- 1020 Lai, Y.-M., Song, S.-R., Lo, C.-H., Lin, T.-H., Chu, M.-F., Chung, S.-L., 2017. Age, geochemical and isotopic  
1021 variations in volcanic rocks from the Coastal Range of Taiwan: Implications for magma generation in the  
1022 Northern Luzon Arc. *Lithos* 272-273, 92-115.
- 1023 Lai, Y.-M., Chu, M.-F., Chen, W.-S., Shao, W.-Y., Lee, H.-Y., Chung, S.-L., 2018. Zircon U-Pb and Hf isotopic  
1024 constraints on the magmatic evolution of the Northern Luzon Arc. *Terrestrial Atmospheric and Oceanic  
1025 Sciences* 29, 149-186.
- 1026 Lee, J.-C., Chu, H.-T., Angelier, J., Hu, J.-C., Chen, H.-Y., Yu, S.-B., 2006. Quantitative analysis of surface  
1027 coseismic faulting and postseismic creep accompanying the 2003, Mw = 6.5, Chengkung earthquake in eastern  
1028 Taiwan. *Journal of Geophysical Research: Solid Earth* 111, B02405. <https://doi.org/10.1029/2005JB003612>.
- 1029 Lee, T.-Q., 1992. Study of the polarity transition record of the upper Olduvai event from Wulochi sedimentary  
1030 sequence of the Coastal Range, eastern Taiwan. *Terrestrial Atmospheric and Oceanic Sciences* 3, 503-518.
- 1031 Lee, T.-Q., Chi, W.-R., 1990. Paleomagnetic dating of the sedimentary formations in the Coastal Range. Special  
1032 Publication of the Central Geological Survey, MOEA 4, 271-294. (in Chinese with English abstract).
- 1033 Lee, T.-Q., Kissel, C., Laj, C., Horng, C.-S., Lue, Y.-T., 1990. Magnetic fabric analysis of the Plio-Pleistocene  
1034 sedimentary formations of the Coastal Range of Taiwan. *Earth and Planetary Science Letters* 98, 23-32.
- 1035 Lee, Y.-H., Byrne, T., Wang, W.-H., Lo, W., Rau, R.-J., Lu, H.-Y., 2015. Simultaneous mountain building in the  
1036 Taiwan orogenic belt. *Geology* 43, 451-454. [https://doi.org/10.1016/0012-821X\(90\)90085-C](https://doi.org/10.1016/0012-821X(90)90085-C).
- 1037 Li, M., 1984. Geology of Ruiyuan Area, Southern Coastal Range, Eastern Taiwan (M.Sc. thesis). National Taiwan  
1038 University, Taipei, Taiwan, 74 pp. (in Chinese).
- 1039 Lin, A.T., Watts, A.B., Hesselbo, S.P., 2003. Cenozoic stratigraphy and subsidence history of the South China Sea  
1040 margin in the Taiwan region. *Basin Research* 15, 453-478.

- 1041 Lin, C.W., Liu, Y.C., Lai, W.C., Cheng, W.H., 1999. Fault tectonics of the Coastal Range, eastern Taiwan. Journal  
1042 of the Geological Society of China 42, 429-446.
- 1043 Lin, S.B., Chen, G.T., 1986. Clay minerals from the Lichi Melange and its adjacent formations in the Coastal Range,  
1044 eastern Taiwan. Acta Geologica Taiwanica: Science Reports of the National Taiwan University 24, 319-356.
- 1045 Lin, W.-H., Lin, C.-W., Liu, Y.C., Chen, P.-T., 2008. Geological Map of Taiwan Scale 1:50,000 - Taitung and  
1046 Jihben Sheet. Central Geological Survey, MOEA, Taiwan, 58 pp. (in Chinese with English abstract).
- 1047 Liou, J.G., Suppe, J., Ernst, W.G., 1977. Conglomerates and pebbly mudstones in the Lichi Melange, eastern  
1048 Taiwan. Memoir of the Geological Society of China 2, 115-128.
- 1049 Lo, H.-J., Chen, W.-S., Song, S.-R., 1993. Geological Map of Taiwan Scale 1:50,000 - Chengkung and Tungho  
1050 Sheet. Central Geological Survey, MOEA, Taiwan, 63 pp. (in Chinese with English abstract)
- 1051 Lundberg, N., Dorsey, R.J., 1988. Synorogenic sedimentation and subsidence in a Plio-Pleistocene collisional basin,  
1052 eastern Taiwan. In: Kleinspehn, K., Paola, C. (Eds.), New Perspectives in Basin Analysis. Frontiers in  
1053 Sedimentary Geology. Springer, New York, pp. 265-280.
- 1054 Lundberg, N., Dorsey, R.J., 1990. Rapid Quaternary emergence, uplift, and denudation of the Coastal Range,  
1055 eastern Taiwan. Geology 18, 638-641.
- 1056 Lundberg, N., Reed, D.L., Liu, C.S., Lieske, J., 1997. Forearc-basin closure and arc accretion in the submarine  
1057 suture zone south of Taiwan. Tectonophysics 274, 5-23.
- 1058 Malavieille, J., Molli, G., Genti, M., Dominguez, S., Beyssac, O., Taboada, A., Vitale-Brovarone, A., Lu, C.-Y.,  
1059 Chen, C.-T., 2016. Formation of ophiolite-bearing tectono-sedimentary mélanges in accretionary wedges by  
1060 gravity driven submarine erosion: Insights from analogue models and case studies. Journal of Geodynamics  
1061 100, 87-103.
- 1062 Malavieille, J., Dominguez, S., Lu, C.-Y., Chen, C.-T., Konstantinovskaya, E., 2021. Deformation partitioning in  
1063 mountain belts: insights from analogue modelling experiments and the Taiwan collisional orogen. Geological  
1064 Magazine 158, 84-103.

- 1065 Mesalles, L., 2014. Mountain Building at a Subduction-Collision Transition Zone, Taiwan - Insights from  
1066 Morphostructural Analysis and Thermochronological Dating (Ph.D. thesis). Université Pierre et Marie Curie,  
1067 Paris, France, 336 pp.
- 1068 Mesalles, L., Lee, Y.-H., Ma, T.-C., Tsai, W.-L., Tan, X.-B., Lee, H.-Y., 2020. A Late-Miocene Yuli belt? New  
1069 constraints on the eastern Central Range depositional ages. *Terrestrial Atmospheric and Oceanic Sciences* 31,  
1070 403-414.
- 1071 Michiguchi, Y., Ogawa, Y., Wakabayashi, J., Dilek, Y., 2011. Implication of dark bands in Miocene–Pliocene  
1072 accretionary prism, Boso Peninsula, central Japan. In: Wakabayashi, J., Dilek, Y. (Eds.), *Mélanges: Processes  
1073 of Formation and Societal Significance*. The Geological Society of America Special Paper 480, pp. 247-260.
- 1074 Moore, G.F., Aung, L.T., Fukuchi, R., Sample, J.C., Hellebrand, E., Kopf, A., Naing, W., Than, W.M., Tun, T.N.,  
1075 2019. Tectonic, diapiric and sedimentary chaotic rocks of the Rakhine coast, western Myanmar. *Gondwana  
1076 Research* 74, 126-143.
- 1077 Nagel, S., Castelltort, S., Garzanti, E., Lin, A.T., Willett, S.D., Mouthereau, F., Limonta, M., Adatte, T., 2014.  
1078 Provenance evolution during arc–continent collision: sedimentary petrography of Miocene to Pleistocene  
1079 sediments in the western foreland basin of Taiwan. *Journal of Sedimentary Research* 84, 513-528.
- 1080 Nemeč, W., 1990. Aspects of sediment movement on steep delta slopes. In: Colella, A., Prior, D.B. (Eds.), *Coarse-  
1081 Grained Deltas*. Special Publication of the International Association of Sedimentologists 10, pp. 29-73.
- 1082 Noda, A., 2016. Forearc basins: Types, geometries, and relationships to subduction zone dynamics. *Geological  
1083 Society of America Bulletin* 128, 879-875.
- 1084 Noda, A., 2018. Forearc basin stratigraphy and interactions with accretionary wedge growth according to the critical  
1085 taper concept. *Tectonics* 37, 965-988.
- 1086 Ogata, K., Mutti, E., Pini, G.A., Tinterri, R., 2012. Mass transport-related stratal disruption within sedimentary  
1087 mélanges: Examples from the northern Apennines (Italy) and south-central Pyrenees (Spain). *Tectonophysics*  
1088 568-569, 185-199.

- 1089 Ogata, K., Mountjoy, J.J., Pini, G.A., Festa, A., Tinterri, R., 2014. Shear zone liquefaction in mass transport deposit  
1090 emplacement: A multi-scale integration of seismic reflection and outcrop data. *Marine Geology* 356, 50-64.
- 1091 Ogata, K., Festa, A., Pini, G.A., Alonso, J.L., 2019a. Submarine landslide deposits in orogenic belts. In: Ogata, K.,  
1092 Festa, A., Pini, G.A. (Eds.), *Submarine Landslides: Subaqueous Mass Transport Deposits from Outcrops to*  
1093 *Seismic Profiles*. John Wiley & Sons, Inc., Hoboken, NJ, USA and American Geophysical Union, Washington,  
1094 D.C., USA, pp. 1-26.
- 1095 Ogata, K., Festa, A., Pini, G.A., Pogačnik, Ž., Lucente, C.C., 2019b. Substrate deformation and incorporation in  
1096 sedimentary mélanges (olistostromes): Examples from the northern Apennines (Italy) and northwestern  
1097 Dinarides (Slovenia). *Gondwana Research* 74, 101-125.
- 1098 Ogg, J.G., 2012. Geomagnetic polarity time scale. In: Gradstein, F.M., Ogg, J.G., Schmitz, M.D., Ogg, G.M. (Eds.),  
1099 *The Geologic Time Scale 2012*. Elsevier, Boston, USA, pp. 85-113.
- 1100 Ooe, G., 1939. Geologic Map of Taiwan, Taito Sheet. Government General of Taiwan, 1-26.
- 1101 Page, B.M., Suppe, J., 1981. The Pliocene Lichi Mélange of Taiwan: its plate-tectonic and olistostromal origin.  
1102 *American Journal of Science* 281, 193-227.
- 1103 Ragan, D.M., 2009. *Structural Geology: An Introduction to Geometrical Techniques*. Cambridge University Press,  
1104 Cambridge, UK, 602 pp.
- 1105 Ramsay, J.G., 1961. The effects of folding upon the orientation of sedimentation structures. *The Journal of Geology*  
1106 69, 84-100.
- 1107 Raymond, L.A., 1984. Classification of melanges. In: Raymond, L.A. (Ed.), *Melanges: Their Nature, Origin, and*  
1108 *Significance*. The Geological Society of America Special Paper 198, pp. 7-20.
- 1109 Raymond, L.A., 2019. Perspectives on the roles of melanges in subduction accretionary complexes: A review.  
1110 *Gondwana Research* 74, 68-89.
- 1111 Reed, D.L., Lundberg, N., Liu, C.-S., Kuo, B.Y., 1992. Structural relations along the margins of the offshore Taiwan  
1112 accretionary wedge: implications for accretion and crustal kinematics. *Acta Geologica Taiwanica: Science*  
1113 *Reports of the National Taiwan University* 30, 105-122.

- 1114 Sandmann, S., Nagel, T.J., Froitzheim, N., Ustaszewski, K., Münker, C., 2015. Late Miocene to Early Pliocene  
1115 blueschist from Taiwan and its exhumation via forearc extraction. *Terra Nova* 27, 285-291.
- 1116 Shyu, C.-T., Chih, M.-C., Hsu, S.-K., Wang, C., Karp, B., 1996. Northern Luzon Arc: Location and tectonic features  
1117 from magnetic data off eastern Taiwan. *Terrestrial Atmospheric and Oceanic Sciences* 7, 535-548.
- 1118 Silver, E.A., Beutner, E.C., 1980. Melanges. *Geology* 8, 32-34.
- 1119 Sinclair, H.D., 2012. Thrust wedge/foreland basin systems. In: Busby, C., Azor, A. (Eds.), *Tectonics of Sedimentary*  
1120 *Basins: Recent Advances*. John Wiley & Sons, Ltd, Chichester, UK, pp. 522-537.
- 1121 Sinclair, H.D., Naylor, M., 2012. Foreland basin subsidence driven by topographic growth versus plate subduction.  
1122 *Geological Society of America Bulletin* 124, 368-379.
- 1123 Song, S.-R., Lo, H.-J., 2002. Lithofacies of volcanic rocks in the central Coastal Range, eastern Taiwan:  
1124 implications for island arc evolution. *Journal of Asian Earth Sciences* 21, 23-38.
- 1125 Song, S.-R., Tang, H.-Y., 2019. Tuff layers in the fore-arc basin of south Coastal Range, eastern Taiwan:  
1126 Implications for volcanic activity and evolution after the arc-continent collision. American Geophysical Union,  
1127 Fall Meeting, 9-13 December, 2019, San Francisco, California, USA. Abstract #V31D-0159.
- 1128 Song, S.-R., Lo, H.-J., Chen, W.-S., 1994. Origin of clastic dikes In the Coastal Range, eastern Taiwan with  
1129 implications for sedimentary processes during the arc-continent collision. *Journal of the Geological Society of*  
1130 *China* 37, 407-424.
- 1131 Stanley, R.S., Hill, L.B., Chang, H.C., Hu, H.-N., 1981. A transect through the metamorphic core of the central  
1132 mountains, southern Taiwan. *Memoir of the Geological Society of China* 4, 443-473.
- 1133 Stow, D.A.V., Mayall, M., 2000. Deep-water sedimentary systems: New models for the 21st century. *Marine and*  
1134 *Petroleum Geology* 17, 125-135.
- 1135 Sun, C.-H., Smith, A.D., Chen, C.-H., 1998. Nd-Sr isotopic and geochemical evidence on the protoliths of exotic  
1136 blocks in the Juisui Area, Yuli Belt, Taiwan. *International Geology Review* 40, 1076-1087.
- 1137 Sung, Q., 1991. Some characteristics of sedimentary blocks in the Lichi Mélange, Coastal Range, Taiwan. *Special*  
1138 *Publication of the Central Geological Survey, MOEA* 5, 231-256. (in Chinese with English abstract).

- 1139 Suppe, J., 1984. Kinematics of Arc-Continent Collision, Flipping of Subduction, and Back-Arc Spreading Near  
1140 Taiwan. *Memoir of the Geological Society of China* 3, 21-33.
- 1141 Suppe, J., Liou, J.G., 1979. Tectonics of the Lichi Mélange and East Taiwan Ophiolite. *Memoir of the Geological*  
1142 *Society of China* 6, 147-153.
- 1143 Tate, G.W., McQuarrie, N., van Hinsbergen, D.J.J., Bakker, R.R., Harris, R., Jiang, H., 2015. Australia going down  
1144 under: Quantifying continental subduction during arc-continent accretion in Timor-Leste. *Geosphere* 11, 1860-  
1145 1883.
- 1146 Teng, L.S., 1979. Petrographical study of the Neogene sandstones of the Coastal Range, eastern Taiwan (I. northern  
1147 part). *Acta Geologica Taiwanica: Science Reports of the National Taiwan University* 20, 129-156.
- 1148 Teng, L.S., 1980. Lithology and provenance of the Fanshuliao formation, northern Coastal Range, eastern Taiwan.  
1149 *Proceedings of the Geological Society of China* 23, 118-129.
- 1150 Teng, L.S., 1981. On the origin and tectonic significance of the Lichi Formation, Coastal Range, eastern Taiwan.  
1151 *Ti-Chih* 3, 51-61. (in Chinese with English abstract).
- 1152 Teng, L.S., 1982. Stratigraphy and sedimentation of the Suilien conglomerate, northern Coastal Range, eastern  
1153 Taiwan. *Acta Geologica Taiwanica: Science Reports of the National Taiwan University* 21, 201-220.
- 1154 Teng, L.S., 1987. Tectostratigraphic facies and geologic evolution of the Coastal Range, eastern Taiwan. *Memoir*  
1155 *of the Geological Society of China* 8, 229-250.
- 1156 Teng, L.S., 1990. Geotectonic evolution of late Cenozoic arc-continent collision in Taiwan. *Tectonophysics* 183,  
1157 57-76.
- 1158 Teng, L.S., Chen, W.-S., Wang, Y., Song, S.-R., Lo, H.-J., 1988. Toward a comprehensive stratigraphic system of  
1159 the Coastal Range, eastern Taiwan. *Acta Geologica Taiwanica: Science Reports of the National Taiwan*  
1160 *University* 26, 19-35.
- 1161 Teng, L.S., Lee, J.C., Hsu, C.B., 2002. Soft-sediment deformation in the Fanshuliao formation of the Coastal Range,  
1162 eastern Taiwan. *Bulletin of the Central Geological Survey, MOEA* 15, 103-137. (in Chinese with English  
1163 abstract).



- 1164 Tensi, J., Mouthereau, F., Lacombe, O., 2006. Lithospheric bulge in the West Taiwan Basin. *Basin Research* 18,  
1165 277-299.
- 1166 Thomas, M.Y., Avouac, J.-P., Gratier, J.-P., Lee, J.-C., 2014. Lithological control on the deformation mechanism  
1167 and the mode of fault slip on the Longitudinal Valley Fault, Taiwan. *Tectonophysics* 632, 48-63.
- 1168 Tripsanas, E.K., Piper, D.J.W., Jenner, K.A., Bryant, W.R., 2008. Submarine mass-transport facies: new  
1169 perspectives on flow processes from cores on the eastern North American margin. *Sedimentology* 55, 97-136.
- 1170 Tsai, M.-C., Yu, S.-B., Shin, T.-C., Kuo, K.-W., Leu, P.-L., Chang, C.-H., Ho, M.-Y., 2015. Velocity field derived  
1171 from Taiwan continuous GPS array (2007 - 2013). *Terrestrial Atmospheric and Oceanic Sciences* 26, 527-556.
- 1172 Wakabayashi, J., 2019. Sedimentary compared to tectonically-deformed serpentinites and tectonic serpentinite  
1173 mélanges at outcrop to petrographic scales: Unambiguous and disputed examples from California. *Gondwana*  
1174 *Research* 74, 51-67.
- 1175 Wang, C.S., 1976. The Lichi Formation of the Coastal Range and arc-continent collision In eastern Taiwan. *Bulletin*  
1176 *of the Geological Survey of Taiwan* 25, 73-86.
- 1177 Wang, J., Li, X., Ning, W., Kusky, T., Wang, L., Polat, A., Deng, H., 2019. Geology of a Neoproterozoic suture:  
1178 Evidence from the Zunhua ophiolitic mélange of the Eastern Hebei Province, North China Craton. *Geological*  
1179 *Society of America Bulletin* 131, 1943-1964.
- 1180 Wang, Y., Chen, W.-S., 1993. Geological Map of Eastern Coastal Range. Central Geological Survey, MOEA,  
1181 Taiwan. (in Chinese with English abstract).
- 1182 Yang, T.F., Tien, J.-I., Chen, C.-H., Lee, T., Punongbayan, R.S., 1995. Fission-track dating of volcanics in the  
1183 northern part of the Taiwan-Luzon Arc: eruption ages and evidence for crustal contamination. *Journal of*  
1184 *Southeast Asian Earth Sciences* 11, 81-93.
- 1185 Yang, T.F., Lee, T., Chen, C.-H., Cheng, S.-N., Knittel, U., Punongbayan, R.S., Rasdas, A.R., 1996. A double island  
1186 arc between Taiwan and Luzon: consequence of ridge subduction. *Tectonophysics* 258, 85-101.
- 1187 Yao, T.M., Tien, P.L., Wang Lee, C.-M., 1988. Clay mineralogical studies on the Neogene formations, Taiyuan  
1188 Basin, southern Coastal Range of Taiwan. *Acta Geologica Taiwanica: Science Reports of the National Taiwan*  
1189 *University* 26, 263-277.

- 1190 Yen, J.Y., Lu, C.H., Dorsey, R.J., Kuo-Chen, H., Chang, C.P., Wang, C.C., Chuang, R.Y., Kuo, Y.T., Chiu, C.Y.,  
1191 Chang, Y.H., Bovenga, F., Chang, W.Y., 2018. Insights into seismogenic deformation during the 2018 Hualien,  
1192 Taiwan, earthquake sequence from InSAR, GPS, and modeling. *Seismological Research Letters* 90, 78-87.  
1193 Yu, S.-B., Chen, H.-Y., Kuo, L.-C., 1997. Velocity field of GPS stations in the Taiwan area. *Tectonophysics* 274,  
1194 41-59.  
1195

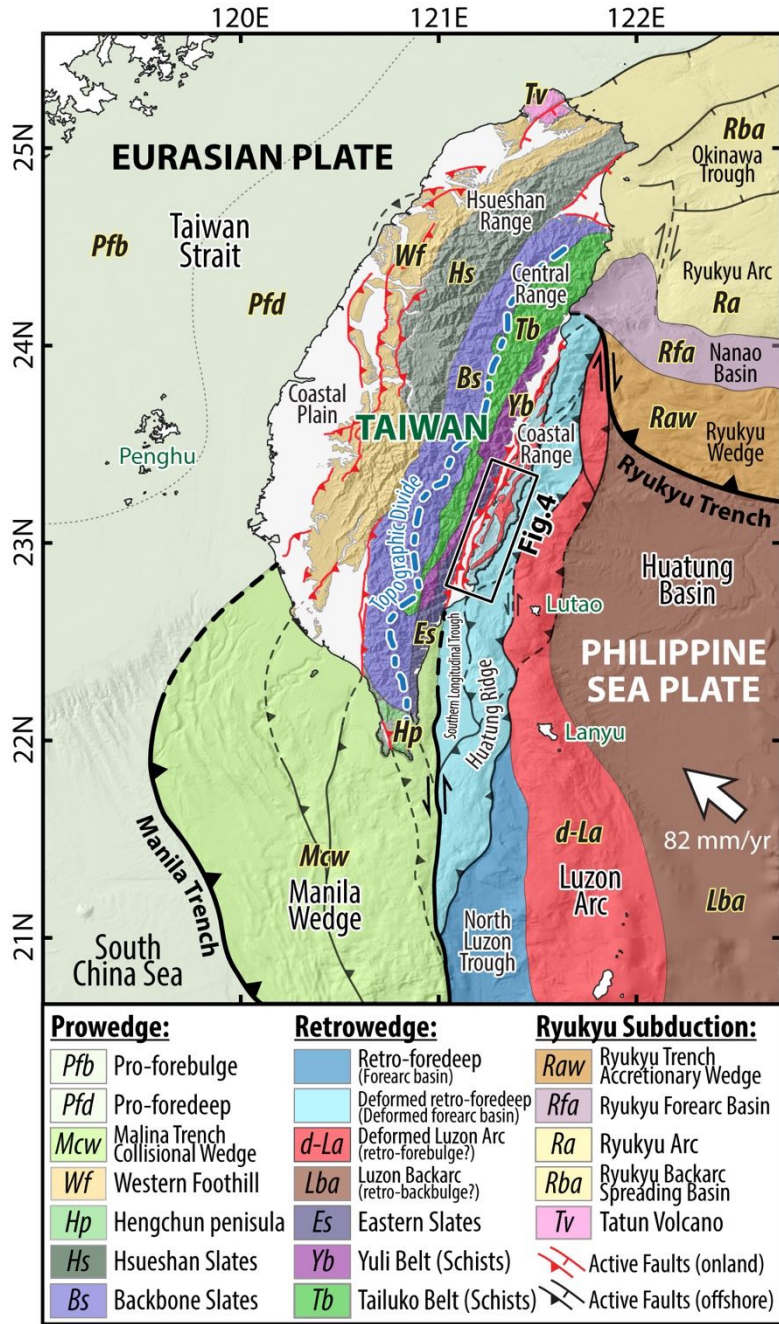


**Figure 1.** Geological setting, Plate configuration and tectonic domains at Taiwan arc-continent collision, synthesized and modified from previous studies (Lin et al., 2003; Huang et al., 2018; Chen et al., 2019; Malavieille et al., 2021).

1196  
1197  
1198  
1199

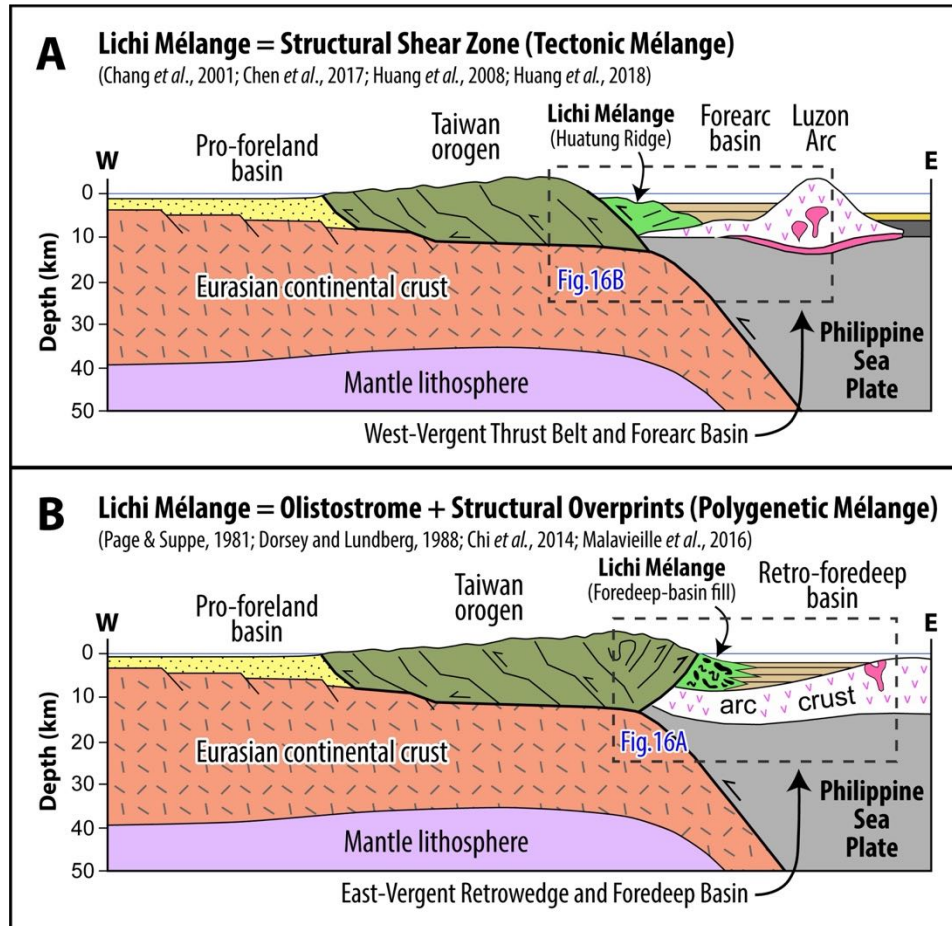
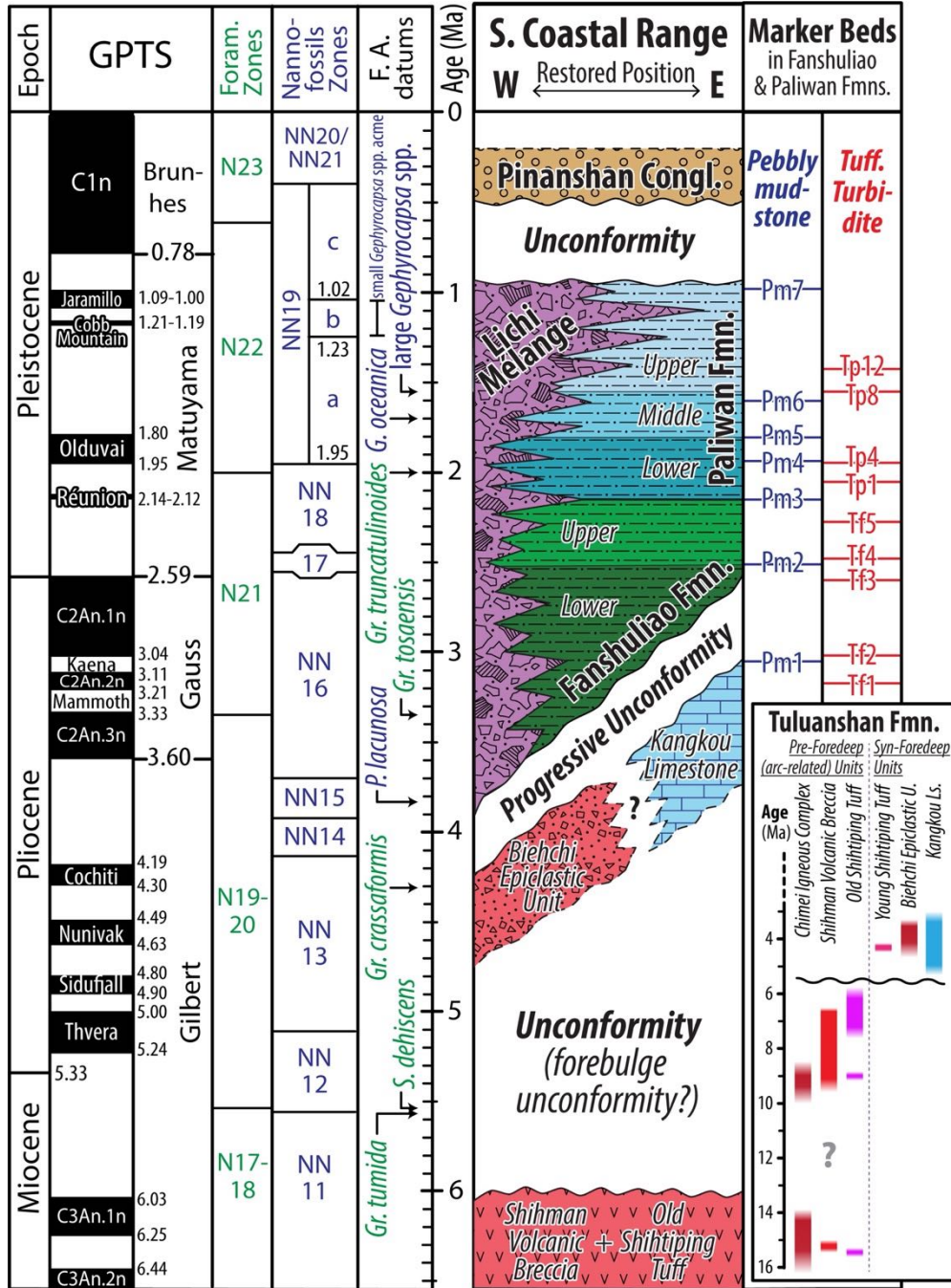


**Figure 2.** Comparison of published models for the origin and tectonic controls on formation of the Lichi Mélange. Figures are identical in the western half (central Taiwan orogen to pro-foreland basin); all differences are expressed in the eastern half, at the complex interface between Eurasian and Philippine Sea plates (dashed box). **(A)** Plate configuration and tectonic domains at Taiwan arc-continent collision, synthesized and modified from Huang *et al.* (2018). **(B)** Lichi Mélange originated as a sequence of marine mega-slumps (olistostromes) formed in a syn-orogenic foredeep basin at the east margin of the east-vergent retrowedge zone of the Taiwan orogen, modified from Malavieille *et al.* (2016).

1200  
 1201  
 1202  
 1203  
 1204  
 1205  
 1206  
 1207  
 1208  
 1209  
 1210  
 1211  
 1212



*\*Chi et al. (1981): exotic blocks in Lichi Mélange are aged ~18-5.6 Ma (NN3-NN11 zone)*

**Figure 3.** Stratigraphic framework of southern Coastal Range (modified from Dorsey, 1992; Lai and Teng, 2016; Lai, L.S.-H. et al., 2018). The geomagnetic polarity timescale (GPTS) and microfossils' first appearance (F.A.) datums of Indo-Pacific region are summarized (Anthonissen and Ogg, 2012; Backman et al., 2012; Ogg, 2012; Chuang et al., 2018). The lower right inset shows ages compiled for the entire Tuluanshan Formation (Huang et al., 1988; Dorsey, 1992; Huang and Yuan, 1994; Chen, 2009; Lai, Y.-M. et al., 2018).

1213  
1214  
1215  
1216  
1217  
1218  
1219



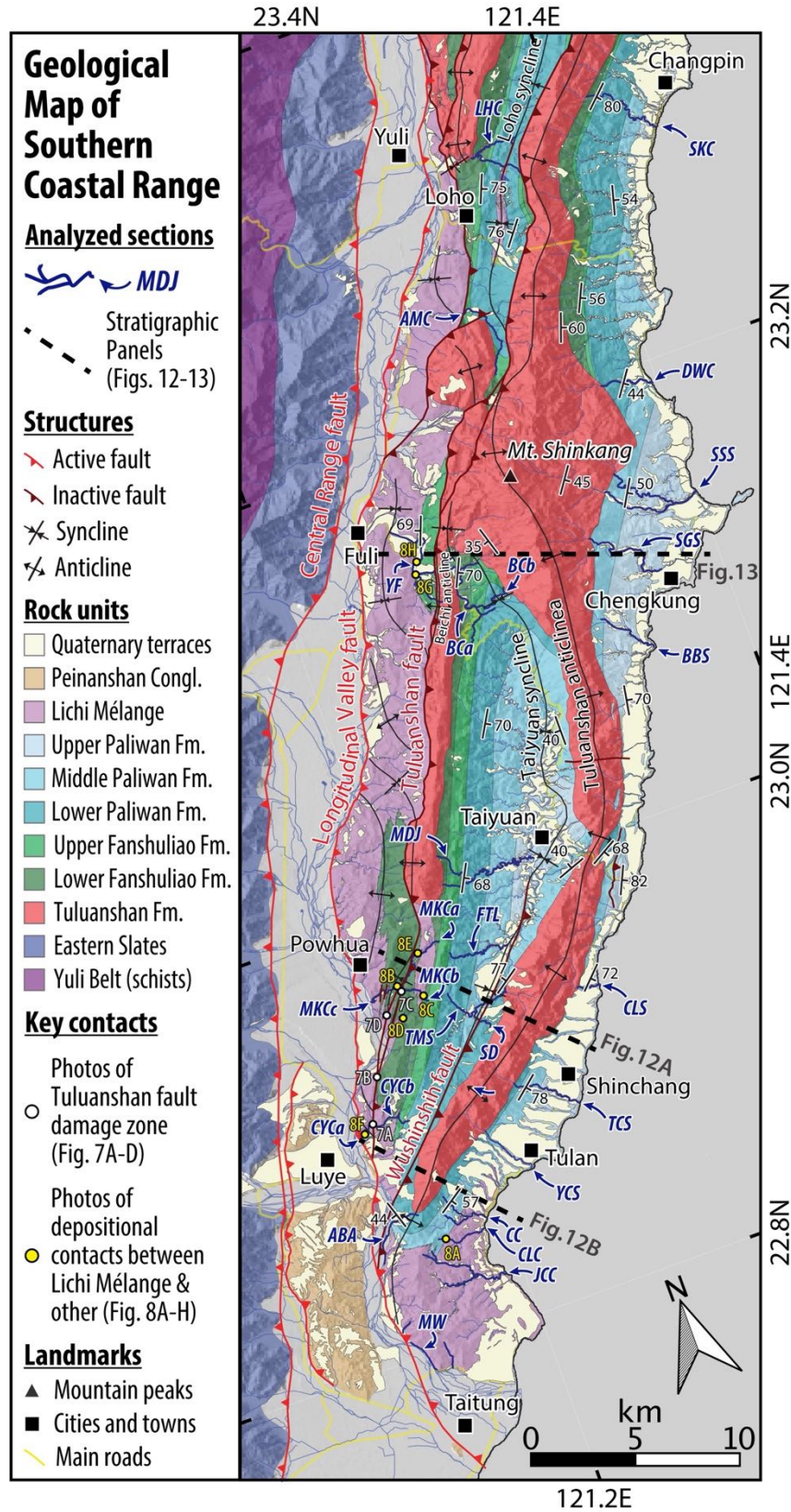


**Figure 4.** Geological map of southern Coastal Range (modified from Wang and Chen, 1993; Lai and Teng, 2016; Lai, L.S.-H. et al., 2018). See detail maps in **Figs. S1-S9**.

1220  
1221  
1222  
1223



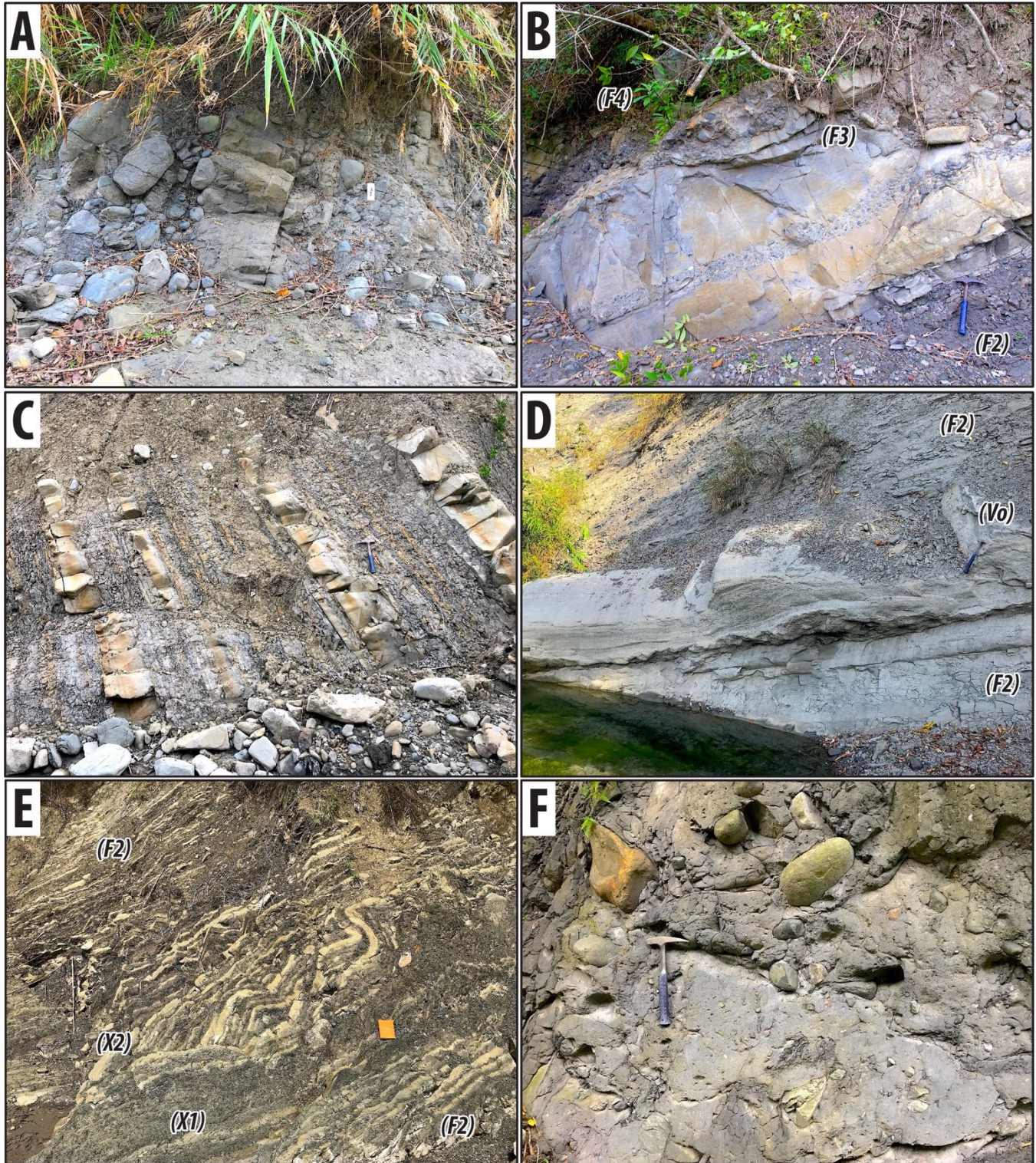


**Figure 5.** Lithofacies photos – I: products of sediment gravity flows. (A) Conglomerate (F4) in Mukeng river – C (MKCc) section. Notes the bedding is overturned; (B) Thick-bedded sandstone and gritstone (F3) in MKCc section, associated with conglomerate (F4) and turbidite (F2); (C) Turbidite (F2) and interbedded mudstone (F1) in Mukeng river – B (MKCb) section; (D) Tuffaceous turbidite (Vo of Tp12), interbeds with orogen-derived turbidites (F2) in Madagida river (MDJ) section; (E) Slump bed (X2) associated with pebbly mudstone Pm1 (X1) and turbidites (F2) in MKCc section; (F) Pebbly mudstone Pm3 (X1) in MDJ section.

1224  
1225  
1226  
1227  
1228  
1229  
1230

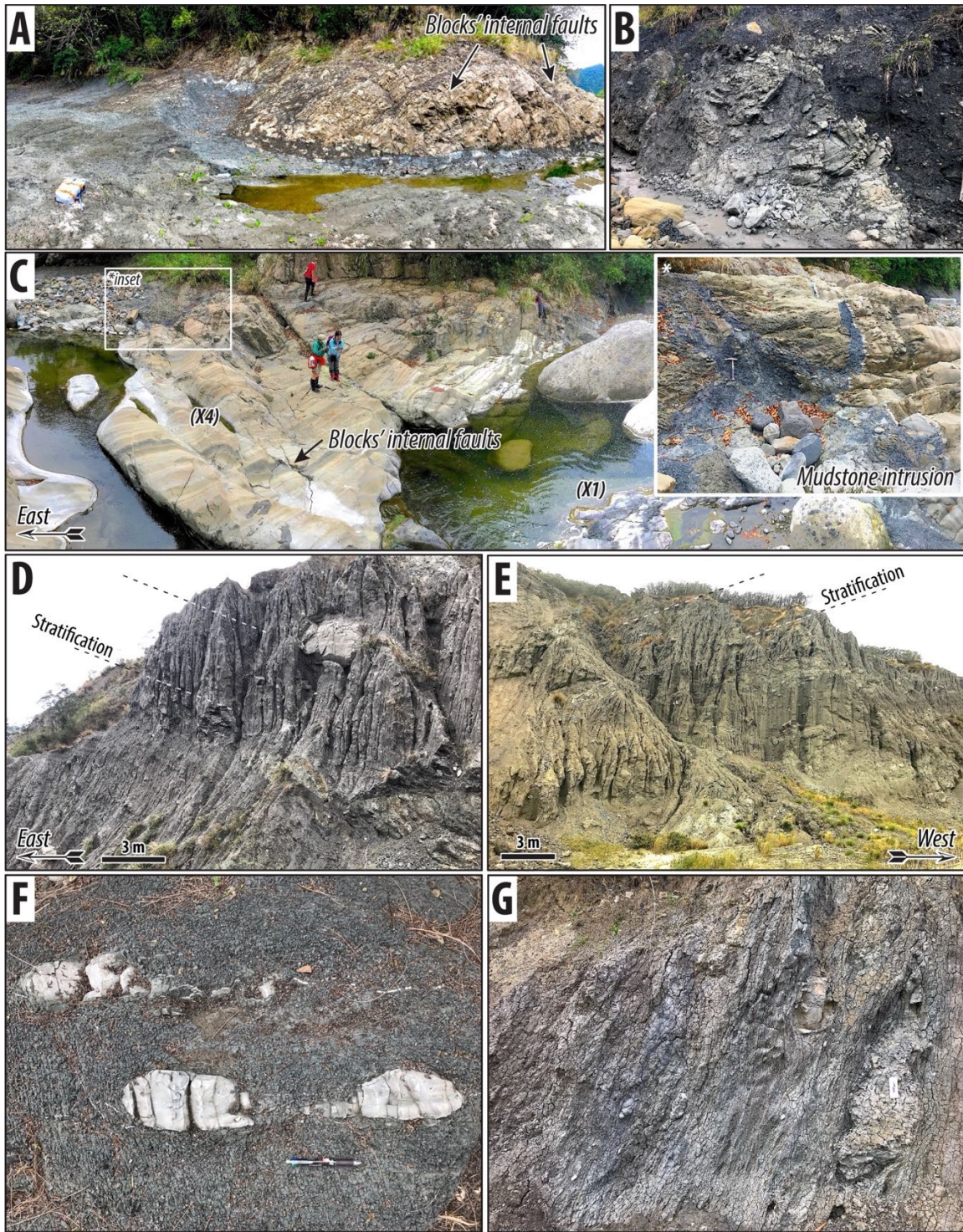
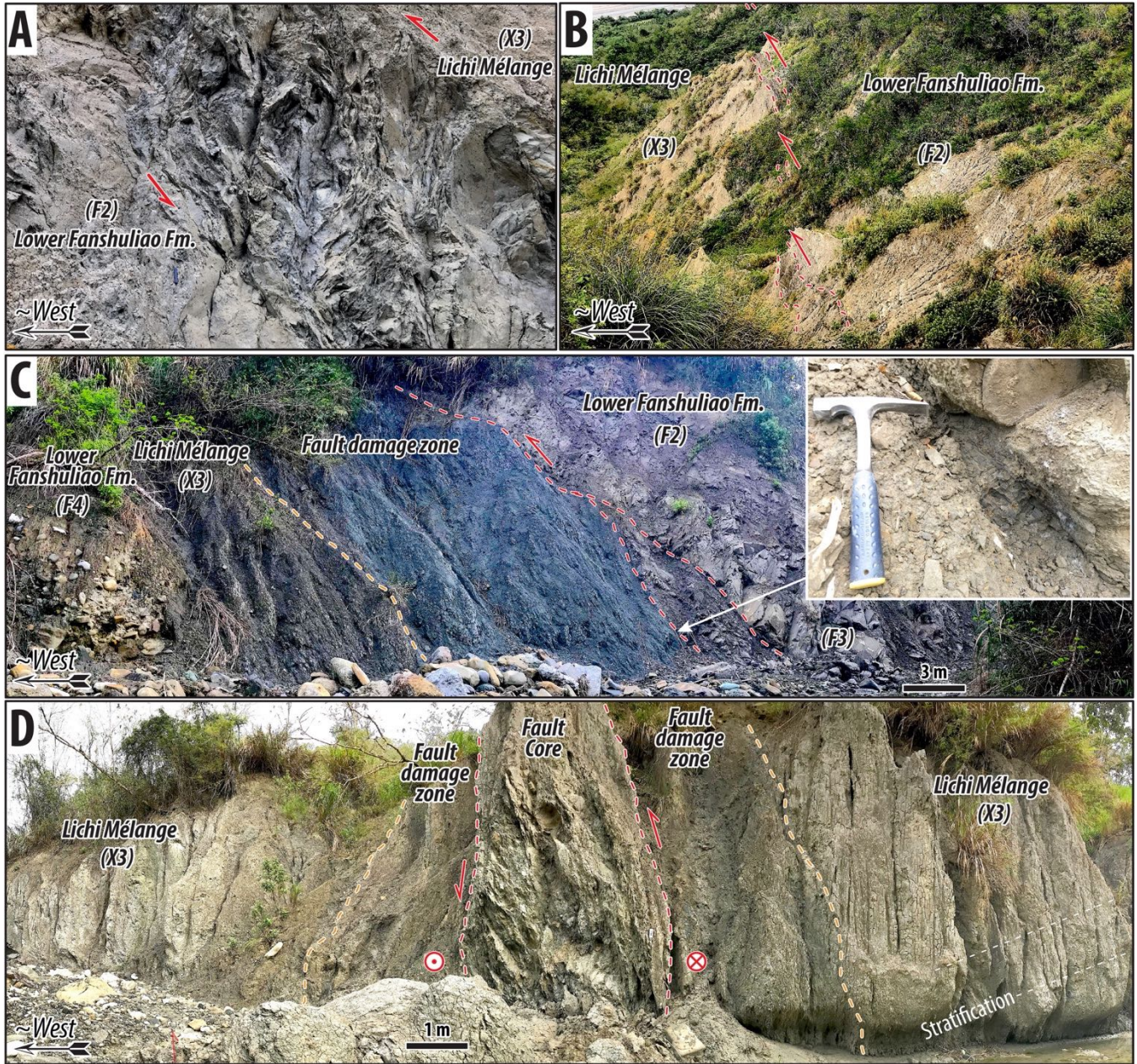


**Figure 6.** Lithofacies photos – II: products of mass wasting. (A) Volcaniclastic (andesitic) sandstone olistoliths (X4) embedded in slump bed (X2) with soft-sediment deformation at Yungfong (YF) section. Notes the internal faults in blocks truncated at blocks' margins; (B) Sandstone olistoliths (X4) with soft-sediment deformation in olistostrome (X3) at Mukeng river – A (MKCa) section; (C) Volcaniclastic (andesitic) sandstone olistoliths (X4) with muddy injectites (inset) in Bieh river – A (BCa) section, associated with pebbly mudstone Pm2 (X1) and slump bed (X2); (D) olistostrome (X3) in Juchiang river (JCC) section with south-dipping stratifications; (E) olistostrome (X3) in Moon World (MW) section with east-dipping stratifications; (F) Sedimentary boudinages in slump bed (X2) at Mukeng river – C (MKCc) section (i.e., broken formation); (G) Scaly foliation and sigmoidal-shaped blocks formed by non-coaxial shear and extensional fracturing (block-in-matrix fabrics) in a sheared horizon near a basal contact of olistostrome (X3) facies at MKCc section.

1231  
1232  
1233  
1234  
1235  
1236  
1237  
1238  
1239  
1240





1241  
1242  
1243  
1244  
1245  
1246  
1247

**Figure 7.** Field photos for Tuluanshan fault damage zone and core (uncompacted cataclasite and/or gouge zone). (A) Tuluanshan fault cataclasite in Chungye river (CYC) section; (B) Gouge zone (bounded by red dash lines) of the Tuluanshan fault along Road no.192; (C) Tuluanshan fault zone in at the base of Mukeng river – B (MKCb) section. The inset shows exposed fault gouge. Pencil cleavage exists in footwall broken formation (Br); (D) Tuluanshan fault zone along Mukengnan river, equivalent to site #19 in Chang et al. (2000). See locations in Fig. 4.

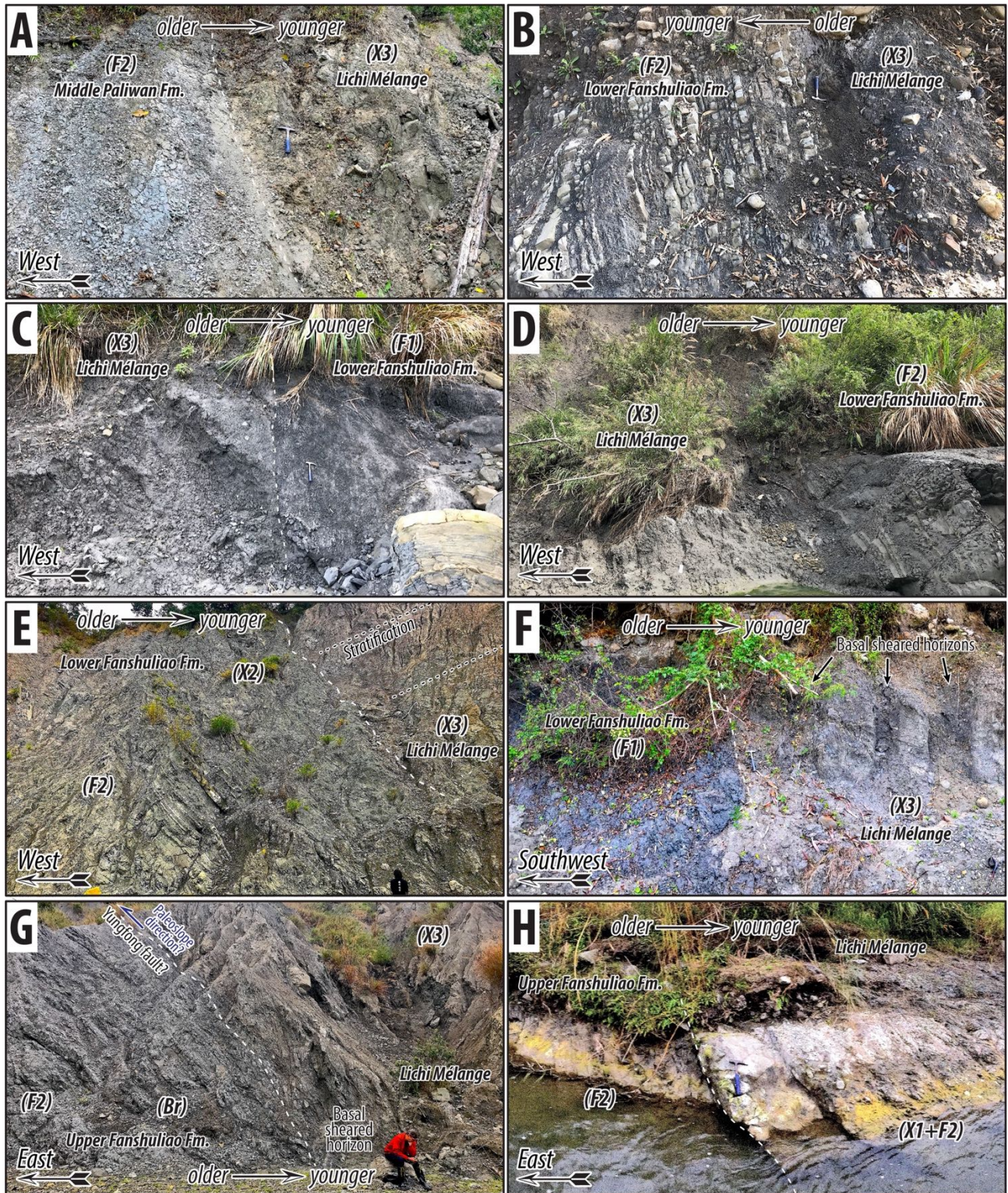


**Figure 8.** Field photos for depositional contacts (white dash lines) between Lichi Mélange & other units. (A) Chiaolai river (CLC) section, same place as ‘Locality J’ in Page and Suppe (1981); (B) Mukeng river – C (MKCb) section. Notes the bedding is overturned; (C) Mukeng river – B (MKCb) section; (D) Mukengnan river section upstream; (E) MKCa section downstream. The stratifications (black dash lines) of olistostrome (X3) appears to onlap on an erosive contact (white dash lines) locally truncating on lower Fanshuliao formation; (F) Chungye river – A (CYCa) section; (G-H) southern and northern contacts of Yungfong (YF) section respectively, which was previously inferred to the “Yungfong fault” (Chen, 1997; Chang et al., 2000). See locations in Fig. 4.

1248  
1249  
1250  
1251  
1252  
1253  
1254  
1255

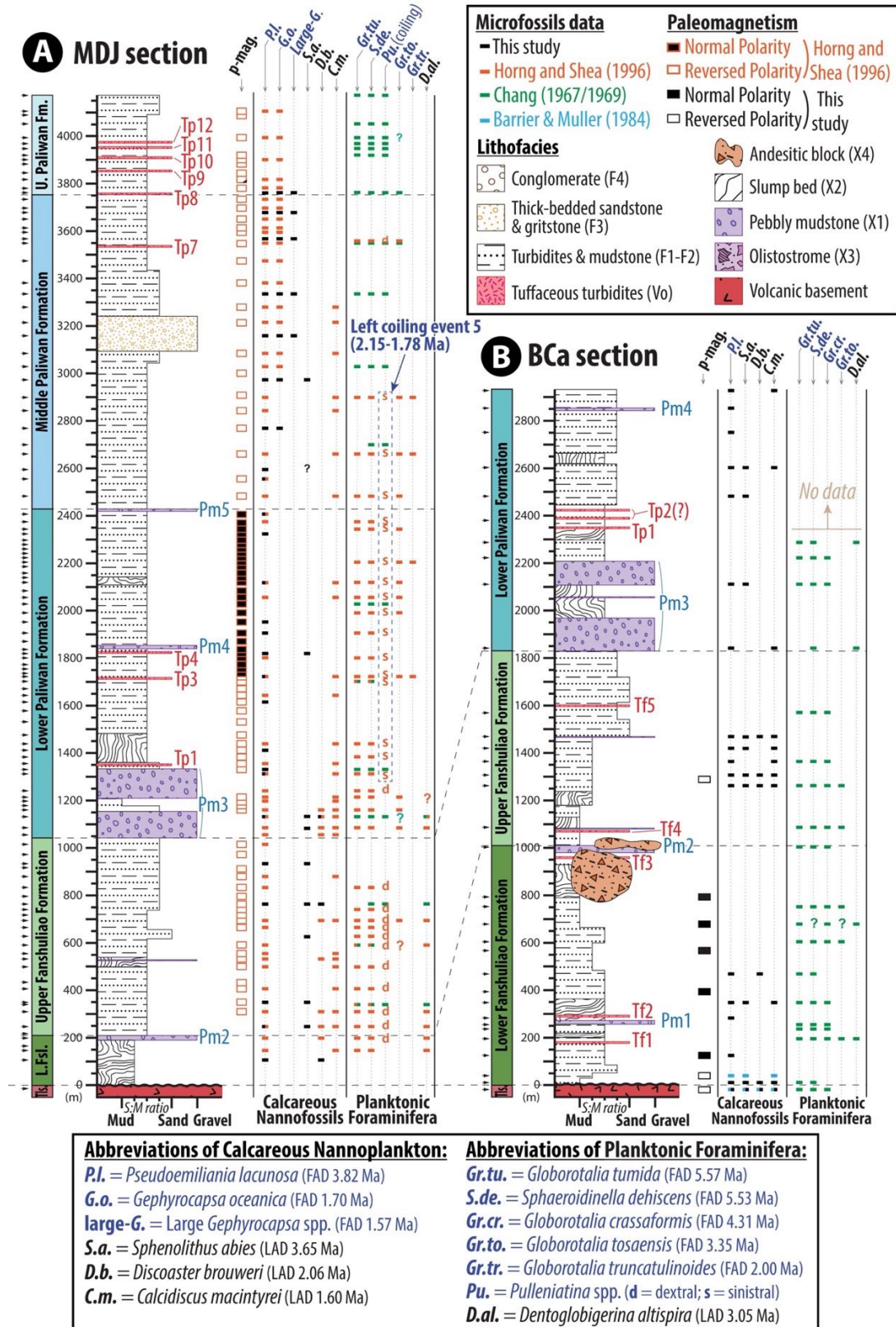
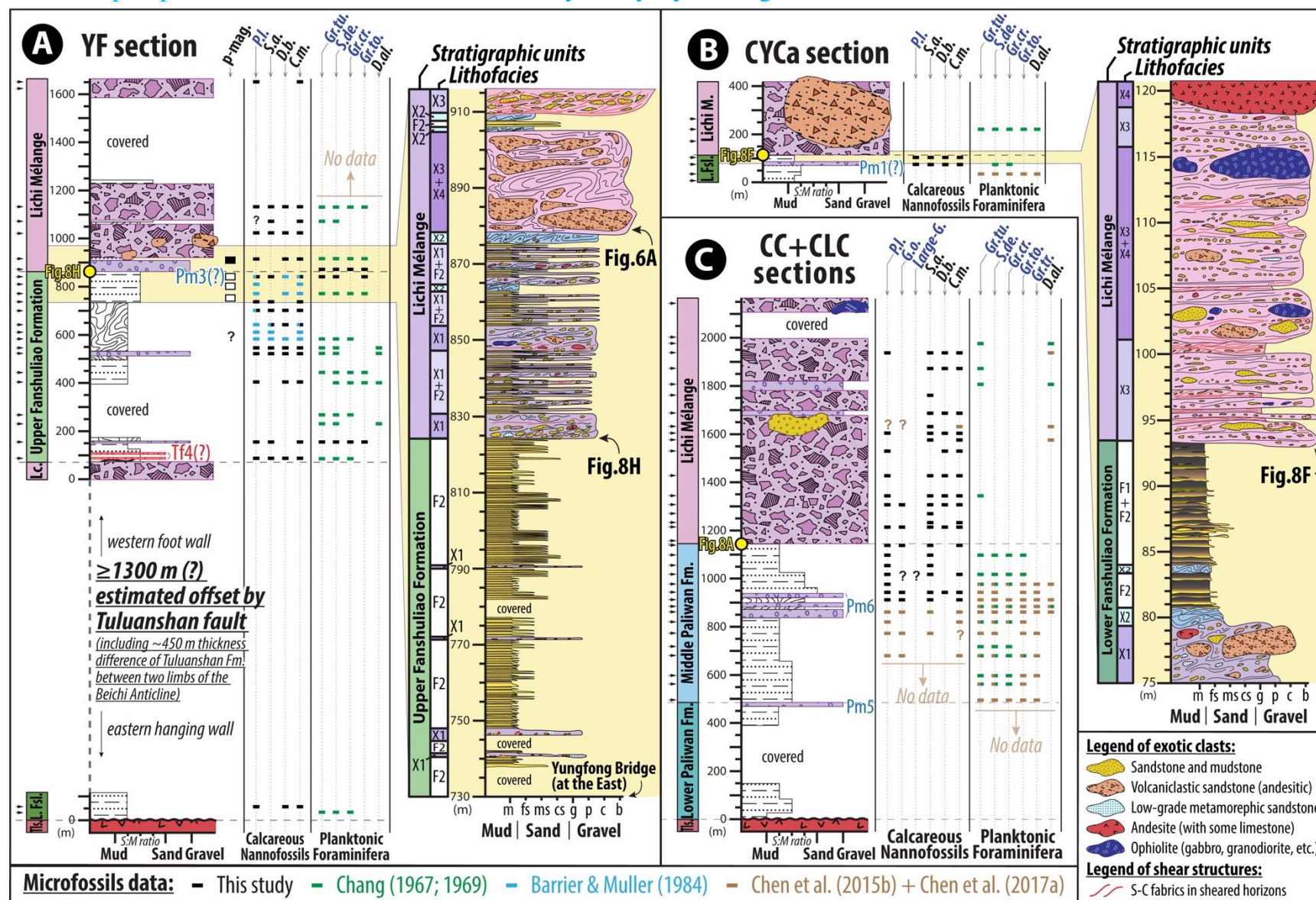


**Figure 9.** Type sections for Fanshuliao and Paliwan formations in the southern Coastal Range. (A) Madagida river (MDJ) section; (B) Bieh river – A (BCa) section. Black arrow heads on the left mark the stratigraphic heights of magneto-biostratigraphic constraints. See detail sample numbers in **Figs. S1, S5, S8, S11** and data in **Tables S3, S5**.

1256  
1257  
1258  
1259  
1260

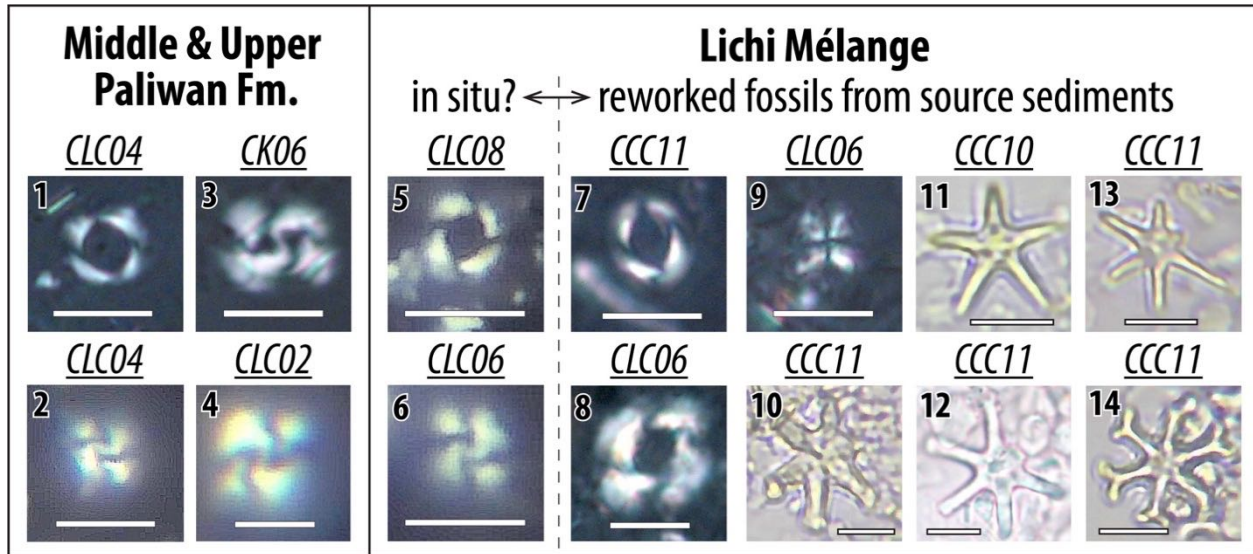




1261  
1262  
1263  
1264  
1265  
1266  
1267

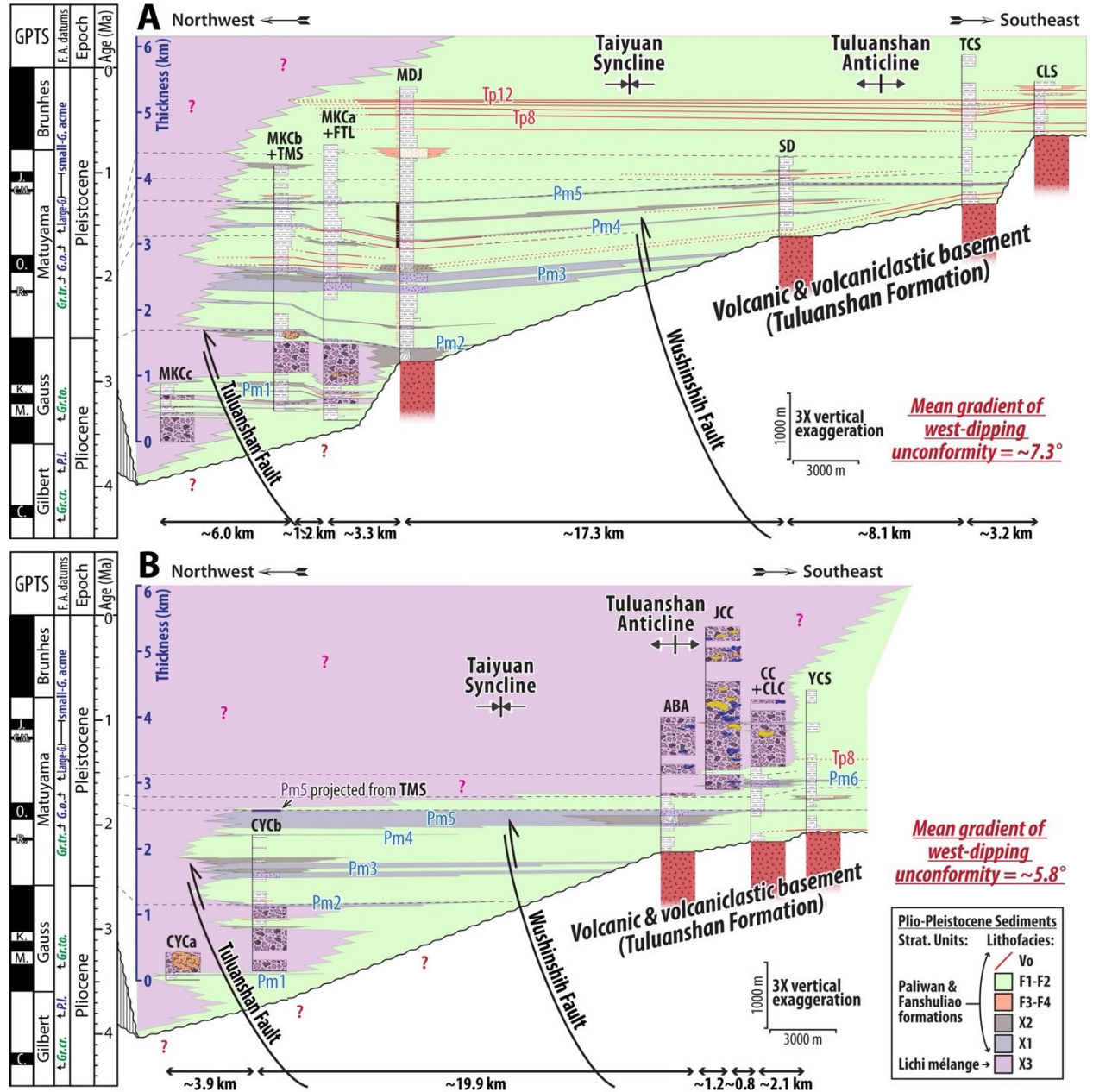
**Figure 10.** Selective sections showing stratigraphic columns and lithofacies changes in the depositional transitions between Lichi Mélange and other sedimentary units. (A) Yungfong (YF) section and measured depositional contact zone; (B) Chungye river - A (CYCa) section and measured depositional contact zone; (C) synthesis of the Chunchie river (CC) and Chiaolai river (CLC) sections. Lithological legends and abbreviation of magneto-biostratigraphy follow Fig. 9. Yellow circles mark the depositional contact zones shown in Figs. 8. Black arrow heads on the left mark the stratigraphic heights where magneto-biostratigraphic constraints exist. See details of sample numbers, microfossils data, and measured contact zone photos in Figs. S12, S13, S15, S16, and Tables S3, S4.

1268



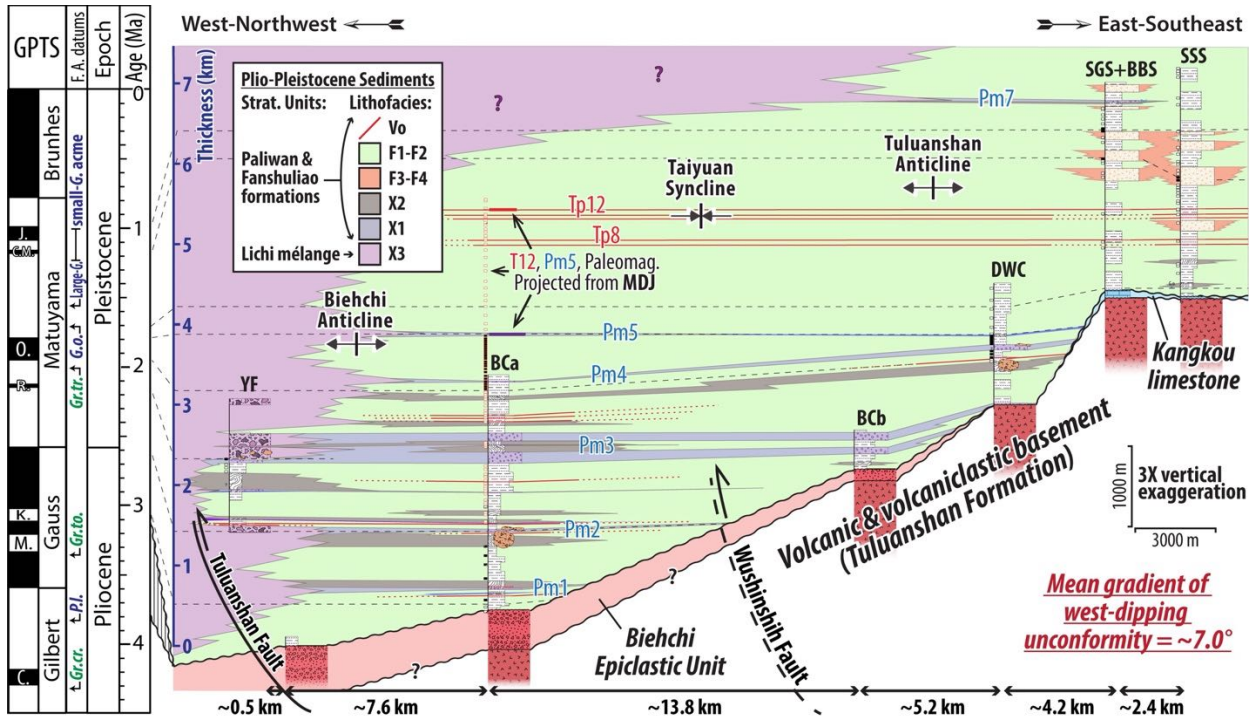
1269  
1270  
1271  
1272  
1273  
1274  
1275  
1276  
1277

**Figure 11.** Polarizing micrographs of index calcareous nannofossils, recovered from Paliwan Formation, and overlying Lichi Mélange, with scale bars of 5  $\mu\text{m}$ . Photo numbers 1 and 5 are *Pseudoemiliana lacunosa*. Numbers 2 and 6 are *Gephyrocapsa oceanica*. Numbers 3 and 4 are large *Gephyrocapsa* sp. Numbers 7 and 8 are medium and large forms of *Reticulofenestra pseudoumbilicus* respectively. Number 9 is *Sphenolithus abies*. Number 10 is *Discoaster druggii* (?). Number 11 is *Discoaster quinqueramus*. Number 12 is *Discoaster surculus*. Number 13 is *Discoaster brouweri*. Number 14 is *Discoaster variabilis*. See sample locations in **Figs S5, S7** and **Table S3**.



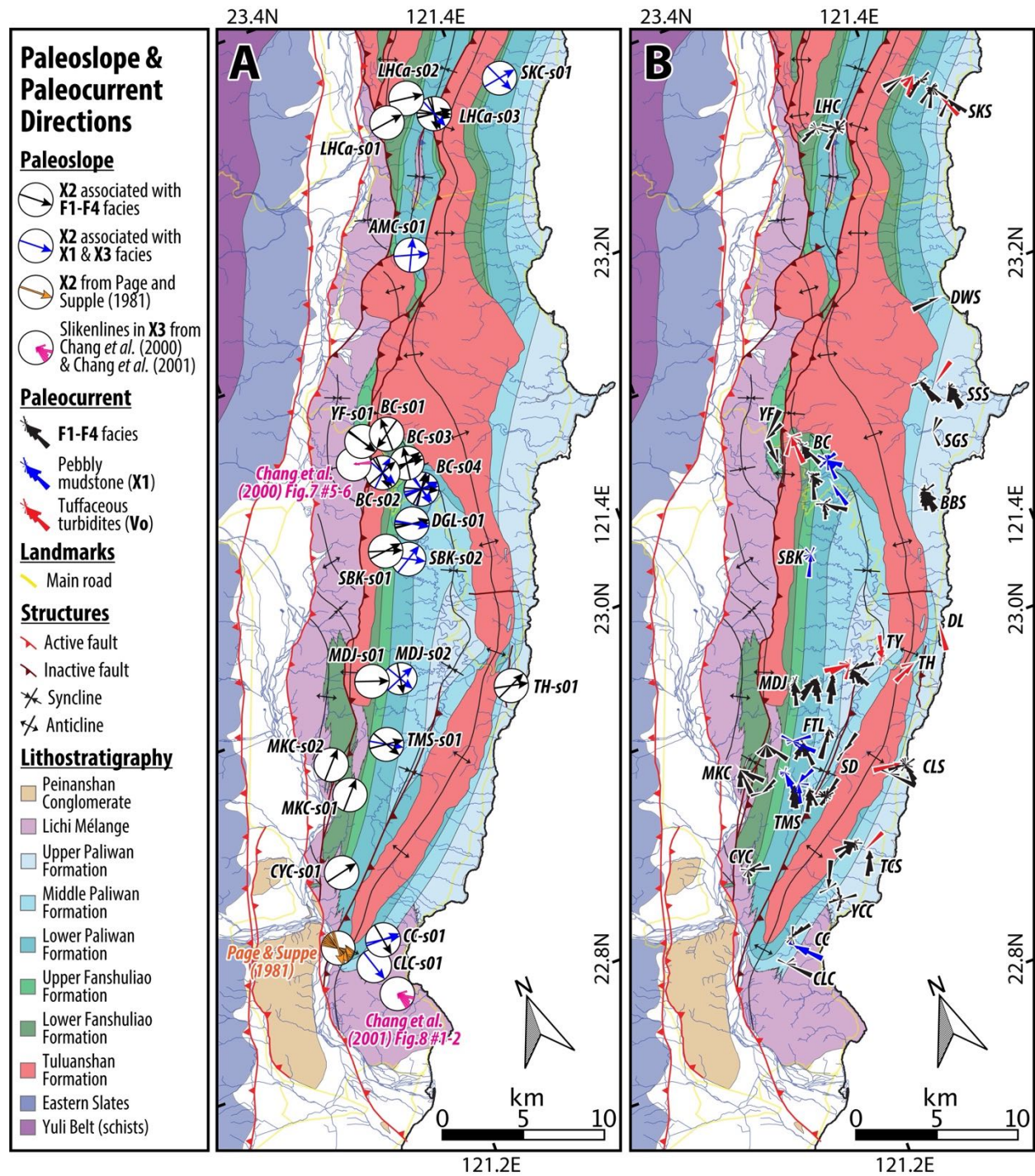
1278  
1279  
1280  
1281  
1282  
1283  
1284

**Figure 12.** Stratigraphic panels of southern Taiyuan area, with restored distances between stratigraphic sections. (A) Powhua-Shinchang transect; (B) Luye-Tulan transect. Black and white rectangles with red outlines along the Madagida river (MDJ) section show paleomagnetic polarities. See locations of transects in Fig. 4. See details of litho-bio-magnetostratigraphic information in Figs. S10-S12.



1285  
1286  
1287  
1288  
1289  
1290  
1291

**Figure 13.** Stratigraphic panel of Fuli-Chengkung area, with restored distances between stratigraphic sections. Black and white rectangles with red outlines show paleomagnetic polarities of Bieh river - A (BCa), Duwei river (DWC), Shingang river (SGS), Babian river (BBS), and Sanshian river (SSS) sections, with data projected from the Madagida river (MDJ) section. See location of the transect in Fig. 4. See details of litho-bio-magnetostratigraphic information in Figs. S12-S14.

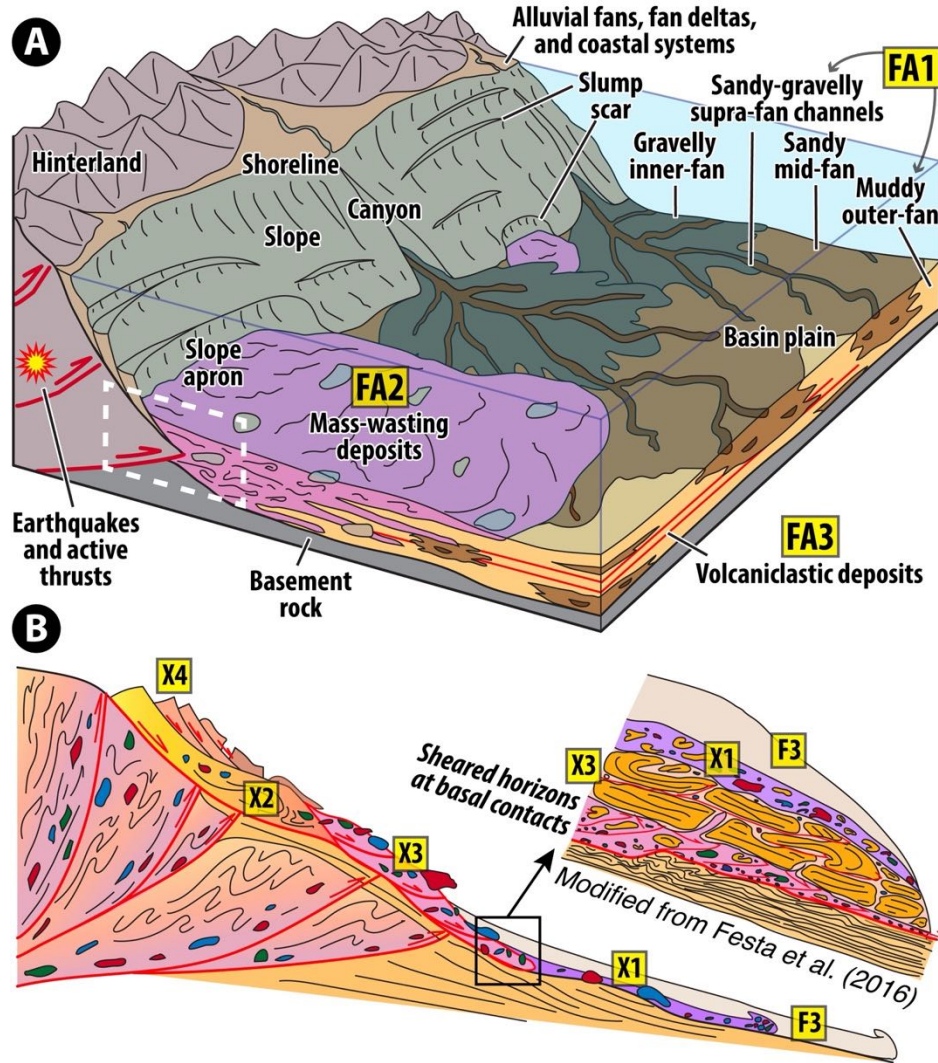


1292  
1293  
1294  
1295  
1296  
1297

**Figure 14.** (A) Inferred paleoslope direction from plunging direction of slump folds (facies X2), including results from Page and Suppe (1981), and bedding corrected east-vergent slikenline shearing sense in basal shear horizons of olistostrome (facie X3) (Chang et al., 2000, 2001); (B) Inferred paleocurrent direction from imbrication, cross-lamination, and flute cast. See method details in text. See raw data, locations, and used structural restorations in the **Tables S1, S2**.







1298  
 1299  
 1300  
 1301  
 1302  
 1303  
 1304

**Figure 15.** Lithofacies classification scheme. (A) Depositional environment model (modified from Stow and Mayall, 2000) and facies associations (FA1-3) of the Coastal Range sedimentary rocks. White dash box marks the place where mélangé-forming processes are portrayed in B; (B) Facies model (modified from Festa et al., 2016; Ogata et al., 2012) for mass-wasting deposits (facies association FA2) and structurally orientated shears (facies association FA3). See detail descriptions of lithofacies and facies associations in **Tables 1, 2**.

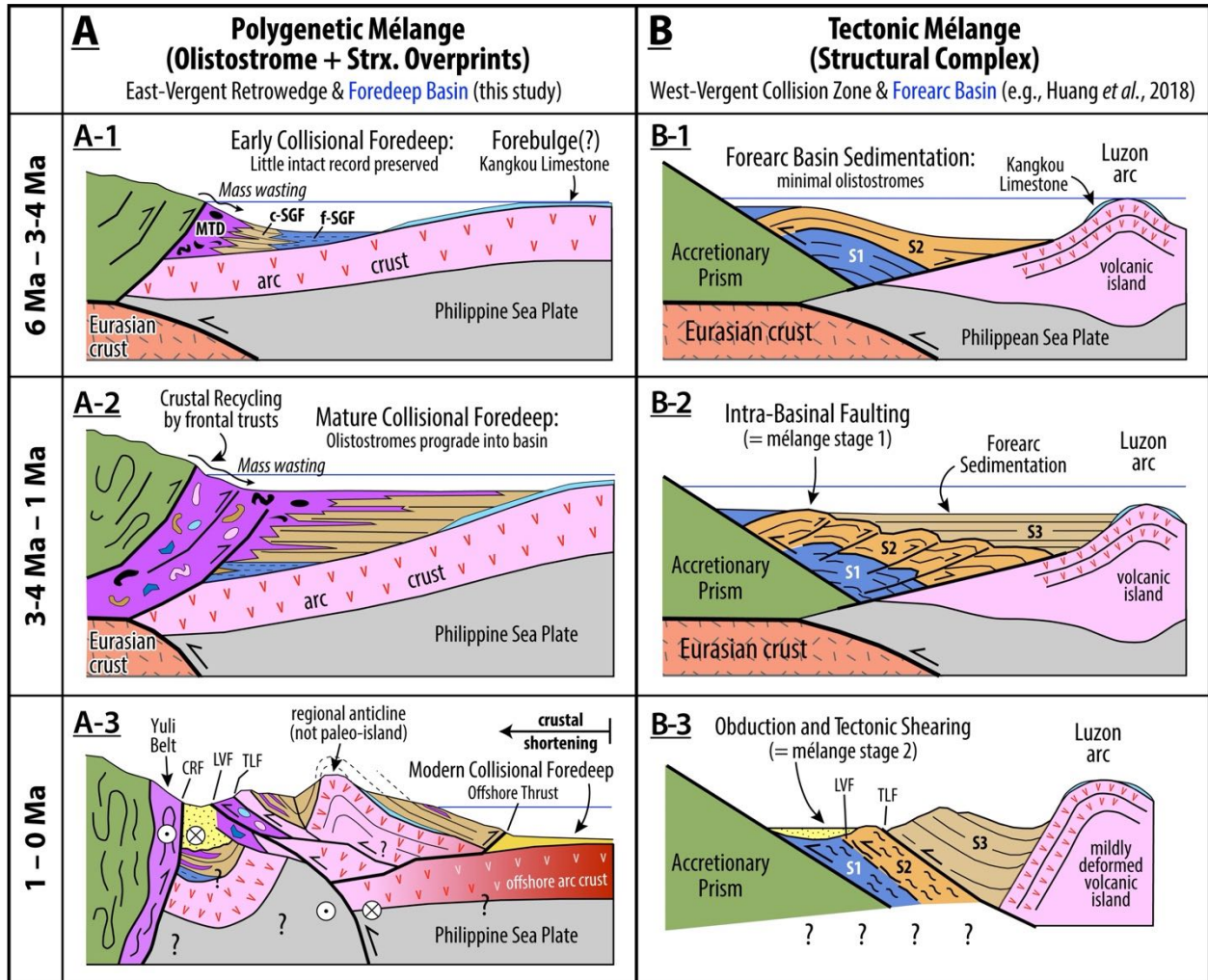


**Figure 16.** Synthetic comparison of the two end-member models interpreting the role, age, and evolution of the Lichi Mélange. (A) Olistostromal origin model. Details are synthesized from several publications (Page and Suppe, 1981; Dorsey and Lundberg, 1988; Chi *et al.*, 2014; Malavieille *et al.*, 2016) and this study. MTD is mass-transport deposits (facies association FA2). Coarse- and fine-grained facies of cohesionless sediment gravity flows (facies association FA1) are marked as c-SGF and f-SGF respectively. CRF is the Central Range Fault (Shyu *et al.*, 2006). LVF is the Longitudinal Valley fault. TLF is the Tuluanshan fault; (B) Tectonic origin model. Figures are modified from Huang *et al.* (2018) which summarized various versions to date. S1 to S3 represent chronostratigraphic sequence 1-3 proposed by Huang *et al.* (2018).

1305  
1306  
1307  
1308  
1309  
1310  
1311  
1312  
1313  
1314

1315 **Table 1.** Lithofacies of sedimentary rocks in the southern Coastal Range. See photos in **Fig. 5-6**.  
1316

Facies Name	Summary Description	Interpreted Processes	Strat. Unit	Mélange Fabric <sup>†</sup>
<b>F1:</b> Mudstone	Dark gray to black mudstone (clay-silt mixture) with rare very thin beds of siltstone to fine-grained sst. Internally structureless to weakly laminated, commonly includes slump zones ~ 0.5 to 5 m thick. Clay is orogen-derived.	Suspension settling	Fsl, Plw	$\alpha$
<b>F2:</b> Turbidites	Sandstone and mudstone in laterally continuous beds. Sst beds ~ 0.01 to 0.5 m thick, normally graded with Bouma sequence, variable sand:mud ratio. Sandstone composition dominantly orogen-derived lithic fragments.	Low-density turbidity current	Fsl, Plw	$\alpha$
<b>F3:</b> Thick-bedded sandstone and gritstone	Normally graded massive to laminated sandstone beds ~ 0.5 to 5 m thick. Granule conglomerate (grit) and pebbly sandstone in lower parts of thicker beds. Large flame and dish structures common near base. Sandstone and clast composition dominated by orogen-derived lithic fragments.	High-density turbidity current	Fsl, Plw	$\alpha$
<b>F4:</b> Conglomerate	Clast-supported conglomerate with pebble to boulder sized clasts, indistinct normal or inverse to normal grading near base. Beds ~1 to 5 m thick. Bases of beds are planar to channelized. Clasts primarily well-rounded low-grade metasandstone and subangular to rounded andesite with trace amounts of mafic rocks (e.g., basalt, gabbro).	Non-cohesive debris flow (grain flow)	Fsl, Plw	$\alpha$
<b>X1:</b> Pebbly mudstone	Matrix-supported, structureless pebbly mudstone in ~ 0.2 to > 300 m thick beds. Bimodal grain-size (mud and gravel), minor sand. Pebble- to boulder-size clasts are angular to subangular andesite & limestone, and subrounded to well-rounded metasandstone and mafic to ultramafic volcanic rocks, unoriented to locally imbricated. Clast-rich and clast-poor zones alternate within single beds. Large flame structures common at base of beds.	Cohesive debris flow or slurry flow	Fsl, Plw	$\alpha?$
<b>X2:</b> Slump bed	Ductilely deformed, convoluted and distorted sedimentary intervals ~ 0.3 to 120 m thick. Local fragmented and dismembered sandstone present in locally sheared matrix (i.e., broken formation) with common structures like pinch-and-swell, ductile to quasi-brittle boudinage, and extensional fractures. Poorly-to-well developed S-C fabrics and scaly foliation observed in less competent fine-grained layers. Protolith is mainly turbidites (F2) with abundant soft-sediment deformation such as micro-faulting and asymmetrically inclined recumbent folds with open to s-shaped fold profile.	Submarine slope failure, slides, and slumps, with sedimentary (gravitational) shearing	Fsl, Plw	$\alpha, \beta, \gamma$
<b>X3:</b> Olistostrome	Laterally extensive zones of chaotic, matrix-supported, unsorted to weakly bedded sedimentary mélange ~ 30 to >500 m thick. Dismembered sedimentary rocks (similar to facies F2) with extra-formational clasts in pervasively deformed fine-grained matrix. S-C fabrics, scaly foliation, and mildly developed slickensides commonly occur in ~1 to 10 meters thick (wide) sheared horizons near the basal contacts, with common structures like pinch-and-swell, ductile to quasi-brittle boudinage, and extensional fractures. Tabular to elongated clasts are aligned parallel to the scaly fabric. Bimodal grain-size (mud and gravel), minor sand. Matrix dominantly gray to moss green clays ("color bands"). Larger clasts display variable rounding. Locally brecciated matrix close to basal shear horizons and cross-cutting faults. Diverse clast compositions: andesite, volcanoclastic sandstone and conglomerate, well-lithified quartz-rich sandstone without orogen-derived lithic fragments, ophiolitic rocks (gabbro, serpentinite, granodiorite, etc.), limestone, metasandstone.	Blocky flow and cohesive debris flow with sedimentary brecciation, shearing, and rock-mixing	Lc	$\delta$
<b>X4:</b> Olistolith	Decimeter- to km-scale single allochthonous block in slumped mudstone. Compositions include andesite, volcanoclastic sandstone and conglomerate, ophiolitic rocks (gabbro, serpentinite, granodiorite, etc.), limestone, and quartz-rich sandstone to low-grade metasandstone. Blocks commonly contain internal brittle shears and fractures with local diapiric mudstone intrusions.	Submarine rock slide or avalanche	Fsl, Plw, Lc	$\alpha?, \delta?$
<b>Vo:</b> Tuffaceous turbidites	White normally graded, planar to ripple-laminated tuffaceous sandstone, with Bouma sequence, in beds ~ 0.01 to 7 m thick. Grain size is silt to very-coarse sand with rare small pebbles near base. Grains are mostly fresh feldspar with locally abundant dark minerals (biotite, pyroxene, hornblende) and volcanic lithic fragments. Minor glass shards at tops of some beds.	Syn-eruptive turbidity current	Fsl, Plw	$\alpha$

1317  
1318 †: We apply the 4-degree ( $\alpha$ - $\delta$ ) classification of stratal disruption (Raymond, 1984), also used in previous studies of the  
1319 Lichi Mélange (e.g., Chang *et al.*, 2000; Chang *et al.*, 2001). Facies abbreviations: F = flysch; X = mélange; Vo = volcanic



1320 **Table 2.** Facies associations of sedimentary rocks in the southern Coastal Range.  
1321

Facies Association	Occurrence and Lithofacies Contacts	Depositional Setting	Rock Unit <sup>†</sup>
<b>FA1:</b> Cohesionless sediment gravity flows	Submarine flysch facies F1 to F4 ( <b>Fig. 5A-C</b> ). F1 = distal basin plain and slope. Base of beds in all facies are typically sharp (erosive). Facies F3 and F4 locally display channelized bases with ~ 2 to 230 m deep and 10's to 100's m wide erosional channels incised into facies F1 and F2.	Proximal to distal submarine fan with supra-fan channels, and distal basin plain.	Fsl, Plw
<b>FA2:</b> Submarine mass wasting and cohesive debris flows	<p>Interbedding, soft-sediment deformation, and lateral transitions among pebbly mudstone (X1), slump bed (X2), and/or olistostrome (X3) (<b>Figs. 5E-F, 6D-E</b>), with randomly distributed lithic blocks (X4) (<b>Fig. 6A-C</b>).</p> <p><b>Observed Basal Contact Styles :</b></p> <p>(1) Base of facies X1, X3, and X4, where resting on FA1, is sharp and erosive (<b>Fig. 8A, 8G</b>), locally with sheared horizons (<b>Fig. 8F-G</b>). Facies X3 locally onlap or downlap onto incised channel margins (<b>Fig. 8E</b>).</p> <p>(2) Base of facies X1 and X3 transitional from X2 (<b>Fig. 5E</b>).</p> <p>(3) Base of facies X1 transitional from thick-bedded sandstone and gritstone (F3).</p> <p>(4) Diapiric intrusions of mixed underlying strata at the margins of X4 (<b>Fig. 6A-C</b>).</p> <p><b>Observed Upper Contact Styles:</b></p> <p>(1) Upper contact of facies X1, X2, X3, and X4 where overlain by facies association FA1 is sharp (<b>Fig. 8B-D</b>).</p> <p>(2) Upper and lateral margins of facies X4 commonly surrounded by facies X1, X2, and X3 (<b>Figs. 6A-E, 10A-B</b>).</p> <p>(3) Upper contact of facies X1 gradually transitional to thick-bedded sandstone and gritstone (F3).</p> <p>(4) Upper contact of facies X3 transitional to X2.</p>	Muddy sediment-rich, mass-transport complex derived from steep slope and deposited at base of slope to proximal basin floor. Local brittle and plastic deformation zones record shearing on discrete basal surfaces of large mass movements. Variable degrees of sediment liquefaction and lubrication that facilitated mass transport.	Lc, Fsl, Plw
<b>FA3:</b> Volcaniclastic deposition	Fresh tuffaceous sandstone beds (Vo) with sharp erosive bases. Primarily interbedded with turbidites (F2), uncommonly preserved where facies other than F2 are dominant ( <b>Fig. 5D</b> ).	Distal syn-eruptive turbidity currents.	Fsl, Plw

1322 †: Abbreviations of stratigraphic units follow **Table 1**.  
1323

